Chemical Engineering Research and Design 209 (2024) 111–131

Contents lists available at ScienceDirect

Chemical Engineering Research and Design

journal homepage: www.elsevier.com/locate/cherd

Modeling and design of a combined electrified steam methane reforming-pressure swing adsorption process

Esther Hsu [a], Dominic Peters [a], Berkay Çıtmacı [a], Parth Chheda [a], Xiaodong Cui [a], Yifei Wang [a], Carlos G. Morales-Guio [a,*], Panagiotis D. Christofides [a,b,*]

[a] Department of Chemical and Biomolecular Engineering, University of California, Los Angeles, CA, 90095-1592, USA
[b] Department of Electrical and Computer Engineering, University of California, Los Angeles, CA 90095-1592, USA

ARTICLE INFO

Keywords:
Steam methane reforming
Electrification
Pressure swing adsorption
Experimental data modeling
Process design
Process operation

ABSTRACT

Steam methane reforming (SMR) is the most widely used hydrogen (H_2) production method, converting natural gas and steam into H_2 and carbon dioxide (CO_2). SMR is a mature industrial technology that burns fossil fuels to provide heat to the endothermic reforming reaction and to generate steam, which contributes to the production of greenhouse gas emissions. In order to reduce heating-based emissions, an electrically-heated steam methane reforming process has been proposed. Conventional SMR uses a packed bed catalyst and receives heat through radiation from hot flames in the surrounding furnace; on the other hand, an electrified SMR employs a washcoated catalyst, and is resistively-heated through the wall of the reactor coil. To gain further insight into the scalability of hydrogen production processes using electrically-heated reformers, this paper takes experimental data from an electrified reformer built at UCLA, extracts kinetic parameters, and uses these parameters to model and scale up a hydrogen production plant with a hydrogen production capacity of 231 kg/h (2607 Nm^3/h). The simulated plant includes a reformer, two water gas shift reactors, pressure swing adsorption (PSA) for separation, and a heat exchange network to make steam for the reformer. A two-column-PSA process is dynamically modeled to output 99% H_2 purity, and the pressures necessary for separation and H_2 recovery are calculated using steady-state simulation data. A sensitivity analysis is conducted for the most energy-efficient H_2 production conditions (e.g., operating pressure, heat flux), and CO_2 production amounts are compared to a conventional SMR process, demonstrating that electrified SMR can potentially be a significantly cleaner alternative. The optimization of electrified reformers must target high mass and heat transfer along the full length of the reformer to achieve near full methane conversion that will minimize off-gas generation from the PSA unit.

1. Introduction

Hydrogen (H_2) has been widely recognized as an ideal energy carrier (Lubitz and Tumas, 2007) that only generates water as exhaust upon combustion or oxidation in a fuel cell. Over 95% of H_2 is currently produced through conventional steam methane reforming (SMR) or coal gasification processes (Panchenko et al., 2023). Depending on the carbon dioxide (CO_2) emissions associated with each H_2 manufacturing process, H_2 is given different color labels. H_2 generated via reforming of natural gas and coal is referred to as grey and brown hydrogen, respectively, to highlight the environmental drawbacks of these production methods. If the accompanying CO_2 is captured and sequestered, then it is labeled as blue H_2. In contrast, green hydrogen, produced from renewable electricity using clean technologies such as water electrolysis, offers a sustainable alternative to the production of carbon-free hydrogen. However, scale-up of green hydrogen production remains limited due to challenges with the scale-up of electrolyzer-based manufacturing plants. Therefore, alternative approaches to reduce the emission of CO_2 associated with the production of H_2 are required. One available strategy is to improve conventional hydrogen production methods through the electrification of the steam methane reforming step.

Steam methane reforming is a net endothermic chemical process that generates H_2 from methane (CH_4) and steam at high temperatures (Bartholomew and Farrauto, 2011). The byproducts, carbon monoxide (CO) and CO_2, must then be separated in an H_2 purification unit. Consequently, a typical SMR-based industrial H_2 production plant typically contains the reforming reactor, the water-gas shift (WGS) reactor, a network of heat exchangers for the cooling of the raw gas and the production of steam, and a gas purification unit (e.g., Molburg and Doctor (2003)).

For the reforming process, conventional SMR plants typically employ multiple reactor coils packed with a nickel-based catalyst, which

* Co-Corresponding authors at: Department of Chemical and Biomolecular Engineering, University of California, Los Angeles, CA, 90095-1592, USA.
E-mail addresses: moralesguio@ucla.edu (C.G. Morales-Guio), pdc@seas.ucla.edu (P.D. Christofides).

https://doi.org/10.1016/j.cherd.2024.07.052
Received 25 June 2024; Received in revised form 23 July 2024; Accepted 24 July 2024
Available online 29 July 2024

are heated by a furnace fueled by the combustion of a portion of the feed (typically natural gas), and the burning of off-gas fuels. The combustion of at least 0.11 kg of methane is required to provide the energy to process 1 kg of methane feed in the reformer when using a steam-to-carbon ratio (S/C) of 3 (Häussinger et al., 2011). As a result, fossil fuel-based heating of the reformer is unsustainable as it leads to significant CO_2 emissions from hydrocarbon combustion. Moreover, heat transfer via radiation from burner flames in the furnace creates non-uniform heat gradients, leading to lower energy utilization, decreased process yields, and lower methane conversion (Kumar et al., 2016). To address these issues, traditional heating can be replaced with electrical resistive heating, also known as Joule-heating, since the heating efficiency for resistively-heated reformers nears 100% (DOE, 1997). At UCLA, an electrically-heated experimental SMR setup was constructed to aid in the development of modeling and control strategies (Çıtmacı et al., 2024a; Cui et al., 2024; Çıtmacı et al., 2024b) that may be integral to the scale-up of this novel reforming method.

The reformer is just one of the units of the SMR plant. The convective section in a conventional reformer generates the much-needed steam to power compression work in the rest of the plant, and also is used to burn and recover energy from the off-gas of the separation unit. Electrification of the radiant section of the reformer requires a new approach to energy integration for the plant and the treatment of off-gases, different from that of conventional hydrogen plants. The design and simulation of H_2 production plants powered by renewable electricity that can achieve high conversion and hydrogen product purity is thus an area of industrial interest. In a hydrogen plant, shift reactors, compressors, and heat exchange networks are needed to achieve better CH_4 conversion and higher H_2 production efficiencies. While these units cannot be practically implemented at experimental scales for purposes of process optimization, they can be simulated using a process simulation software provided that the mathematical models for transport, reaction, and separation in the different units are experimentally validated.

After achieving nearly complete conversion of CH_4 and CO during the electrified reforming process and shift reactors, the H_2 effluent requires further purification via separation processes. Since steam can be condensed at room temperature, the removal of other gases, particularly CO_2, must be considered. Hence, methods for H_2 purification need to be used. Specifically, common approaches for H_2 purification involve membrane separation, metal hydride separation, cryogenic distillation, chemical absorption (Wang et al., 2024; Du et al., 2021), and pressure swing adsorption (PSA). With the development of membrane technologies, H_2-selective membranes and CO_2-selective membranes have been utilized for H_2 purification. However, disadvantages such as expensive costs (Sazali, 2020a), poor selectivity (Li et al., 2015), and fragility (Sazali, 2020b) make it challenging to implement these new membrane materials in an industrial setting. For metal hydride separation, many metallic hydride materials such as MgH_2, $LiAlH_2$, $NaAlH_4$, $Mg(AlH_4)_2$, $LiBH_4$, and AlH_3 have been developed (Klopčič et al., 2023). Furthermore, Dunikov et al. (2016) successfully separated H_2/CO_2 mixtures by using AB_5-type hydride alloys. However, some major disadvantages (Klopčič et al., 2023), involving poor reversibility, high cost, and slow kinetics have to be dealt with before applying these metal hydride membrane materials to industrial practices. For purification via cryogenic distillation, H_2 gas can be separated from other hydrocarbons like ethane and ethylene based on the difference in the volatilities of each gas species (Song et al., 2019; Du et al., 2021). However, CO_2 cannot be removed from H_2 mixtures during cryogenic distillation, as it forms solids at extremely low temperatures. Chemical absorption using absorbents like liquid monoethanolamine (MEA) is also available for large-scale H_2 purification (Wang et al., 2024), and many chemicals have been discovered as proper absorbents. For example, Ivanov et al. (2017) suggested removing CO_2 from hydrogen mixtures using methyldiethanolamine (MDEA). Unfortunately, a high H_2 purity (99% or higher) cannot be usually obtained by solely using an amine absorber (Luberti and Ahn, 2022; Wang et al., 2024), and in addition to the large consumption of steam required for solvent regeneration, an additional PSA unit is required to increase the purity of the H_2 product (Luberti and Ahn, 2022).

PSA is a well-established technology for gas separation, applied in various fields such as gas drying, air separation, and H_2 purification (e.g., Grande (2012)). Similar to other adsorption separation processes, PSA involves two basic steps (Ruthven et al., 1996). The first step is adsorption, where the species desired to be separated is/are adsorbed by a dedicated adsorbent. The second step is regeneration or desorption, where the adsorbed species is/are removed from the adsorbent to regenerate the adsorbent. Notably, the regeneration step in PSA relies on reducing the bed pressures to remove adsorbed species, which is a fundamental feature of PSA (Ruthven et al., 1996). In terms of separation technologies, PSA can be categorized into single-bed and multi-bed systems based on the number of adsorbers (Wiheeb et al., 2016). Single-bed PSA typically has a shorter cycle time and larger pressure drop, whereas multi-bed PSA is suitable for continuous feed and product flow (Wiheeb et al., 2016). Considering the continuous feed flow during H_2 production, a multi-bed PSA is chosen for H_2 purification.

In this work, a reformer model is built on experimental data generated by UCLA's electrically-heated steam methane reformer. This model is used within an Aspen simulation environment to simulate a scaled-up version of the plant with a hydrogen production capacity of 231 kg/h, which is closer to industrial production levels. A second Aspen Plus model is developed which includes a full plant model with shift reactors, and PSA for separation. In particular, the PSA process is carried out using an extended Langmuir model in the Aspen Adsorption software. Finally, a sensitivity analysis is carried out to determine the impact of key operating variables on the overall energy consumption and compare the conventional SMR process versus the electrified SMR process.

2. Nomenclature

- a: Specific outer surface area of the catalyst. [m^2 m^{-3}]
- Bo: Bodenstein number, the ratio between the axial dispersion time and the mean residence time. Dimensionless variable. [-]
- $C_{CH_{4,inlet}}$: Concentration of methane at the inlet of steam methane reformer. [mol m^{-3}]
- C_i: Concentration of species i. [mol m^{-3}]
- D_{ax}: Axial dispersion coefficient in the reactor. [m^2 s^{-1}]
- Da_{II}: Second Damkhöler number, the ratio of the characteristic mass transfer time and the characteristic reaction time. Dimensionless variable. [-]
- d_h: Hydraulic diameter of the reactor tube. [m]
- D_m: Molecular diffusivity. [m^2 s^{-1}]
- d_p: Adsorbent particle diameter. [m]
- d_t: Diameter of the reactor. [m]
- ϵ_i: Inter-particle voidage. [m^3_{void} m^{-3}_{bed}]
- eff_{Energy}: Reformer energy conversion efficiency. [-]
- HHV_i: Higher heating value of gas species i. [J/mol]
- $IP_{1,i}$: Extended Langmuir isotherm coefficient. [mol kg^{-1} for i = CH_4, CO, CO_2, and H_2]. The kg unit in the denominator refers to the mass of activated carbon.
- $IP_{2,i}$: Extended Langmuir isotherm coefficient. [mol K^{-1} kg^{-1} for i = CH_4, CO, CO_2, and H_2]. The kg unit in the denominator refers to the mass of activated carbon.
- $IP_{3,i}$: Extended Langmuir isotherm coefficient. [bar^{-1} for i = CH_4, CO, CO_2, and H_2]
- $IP_{4,i}$: Extended Langmuir isotherm coefficient. [K for i = CH_4, CO, CO_2, and H_2]
- k_G: Global mass transfer coefficient for a catalytic wall multichannel reactor. [m s^{-1}]

- K_i: Adsorption constant of gas species i. [Pa^{-1} for i = CH_4, H_2, CO and unitless for i = H_2O]
- K_j: Equilibrium constant for reaction j. [Pa^2 for j = 1 (SMR reaction), unitless for j = 2 (WGS reaction)]
- k_j: Reaction rate constant of reaction j. [mol $Pa^{0.5}$ $(kg_{cat}\ s)^{-1}$ for j = 1 (SMR reaction), mol Pa^{-1} kg_{cat}^{-1} s^{-1} for j = 2 (WGS reaction)]
- k_m: Mass transfer coefficient. [m s^{-1}]
- L_t: Length of the reactor. [m]
- MTC_i: Mass transfer coefficient of species i. [1/s for i = CH_4, CO, CO_2, and H_2]
- $\dot{n}_{H_2,Out}$ and $\dot{n}_{H_2,In}$: Molar rate of hydrogen in the outlet and inlet of the reformer. [mol/s]
- $\dot{n}_{CH_4,In}$: Molar rate of methane in the inlet of the reformer. [mol/s]
- n_i: Dynamic adsorption amount of the species i [mol kg^{-1} for i = CH_4, CO, CO_2, and H_2]
- n_i^*: Equilibrium adsorption of species i. [mol kg^{-1} for i = CH_4, CO, CO_2, and H_2]
- P_i: Partial pressure of gas species i. [Pa for i = CH_4, CO, CO_2, and H_2]
- ρ_g: Density of the gas species i in the reactor. [kg m^{-3}]
- r_{net}: Net reaction rate for the steam methane reformer. [mol kg^{-1} s^{-1}]
- r_1^{SMR}, r_2^{WGS} and r_2^{HT-WGS}, r_2^{LT-WGS}: Rates of steam methane reforming reaction, water gas shift reaction in the reformer, the high-temperature shift reactor and the low-temperature shift reactor. [mol kg^{-1} s^{-1}]
- R: Universal gas constant [J mol^{-1} K^{-1}]
- Re: Reynolds number. Dimensionless variable. [-]
- Sc: Schmidt number, the ratio of momentum (viscous) diffusion to molecular diffusion. Dimensionless variable. [-]
- Sh_∞: Asymptotic Sherwood number for constant concentration. Dimensionless variable. [-]
- Sh'_∞, Sh''_∞: Asymptotic Sherwood number at constant mass flow (with zeroth-order reaction) from the bulk to the wall, for mass transfer with chemical reaction. Dimensionless variables. [-]
- T: Reactor temperature. [K]
- t_m: Characteristic mass transfer time. [s]
- t_r: Characteristic reaction time. [s]
- u: Linear velocity through the reactor. [m s^{-1}]
- v_g: Fluid superficial velocity. [m s^{-1}]
- z: Axial length of PSA columns. [m]
- μ: Dynamic viscosity. [kg m^{-1} s^{-1}]
- χ: Geometric factor used in calculating the Bo number. [-]

3. Modeling of electrified steam methane reforming process via aspen

The objective of the first part of this work is to simulate the electrically-heated steam methane reforming-based H_2 production plant using process simulators to examine the impact of key process parameters. In this process, H_2 is produced by the reaction of methane and steam flow to the reactor, as shown in Eq. (1), which presents the steam methane reforming reaction (Eq. (1a)) and the water gas shift reaction (Eq. (1b)):

$$\text{Steam methane reforming}: CH_4 + H_2O \rightleftharpoons 3H_2 + CO, \quad \Delta H_{298} = 206.1\ \text{kJ mol}^{-1} \tag{1a}$$

$$\text{Water gas shift}: CO + H_2O \rightleftharpoons CO_2 + H_2, \quad \Delta H_{298} = -41.15\ \text{kJ mol}^{-1} \tag{1b}$$

3.1. Process overview

The proposed steam methane reforming-based H_2 production plant is simulated using Aspen Plus V12 and is in accordance with the process proposed by Do et al. (2023). The simulation can be divided into three main sections which are the electrified steam methane reforming (e-SMR) process, water gas shift reactors, and the pressure swing adsorption section. The operational parameters for the sections have been defined in Table 1. The e-SMR is simulated as a plug flow reactor (PFR) using the *RPLUG* reactor block. In Aspen, *RPLUG* is employed as a rigorous catalytic simulation block with LHHW kinetic equations based on the plug flow kinetic parameters by Xu and Froment (1989) and catalyst weight. This simulation is discretized and solved in the axial domain, and the LHHW kinetic model incorporated in the *RPLUG* simulation block for the reformer was experimentally validated. The CH_4 stream is compressed using a three-stage compressor with an intercooling temperature ratio of 0.85. All stages are set to the same pressure ratio and compressed CH_4 is mixed with steam. The e-SMR is assumed to run on electricity derived from renewable sources, which further reduces upstream CO_2 emissions.

For the reformer section of the overall process simulation (see Fig. 1), heat transfer must be accounted down the length of the reformer since the SMR reactions generate and consume varying amounts of heat at different axial positions. Thus, the reforming unit needs the correct energy information to adequately model the composition and kinetic profiles along the length of the reformer, and this work discusses two different approaches to energy modeling in the reformer section of the simulation. The first approach is explained in this section and involves programming a heat flux profile down the length of the reactor to match the experimental thermocouple measurements in the same positions (13.5 cm and 34.25 cm from the outlet of the reformer). Given that the experiments only have two thermocouples, the experimental energy information is limited, and the heat flux profiles that are programmed into Aspen are approximations of the true energy distribution. The programmed heat flux profiles are not unique and can be programmed in a variety of ways. The lab-scale simulation in Fig. 1 contains discrete-valued flux profiles that make physical sense under the notion that the endothermic reforming reaction requires a significant heat of reaction at the beginning of the reformer tube. The second approach, discussed in Section 3.2, selects an average heat flux for the entire reactor that provides the desired steady-state temperature at the outlet of the reformer. The second approach is needed for the SMR scale-up procedure because the temperature and flux profiles for an electrically heated, washcoated reformer at elevated pressures and space velocities are experimentally unknown. To our knowledge, this is the first experimentally validated Aspen model for a Joule-heated reformer with a Ni/ZrO_2 washcoated catalyst at 1 bar and 5 bar.

The reformer section focuses on H_2 production according to Eq. (1a), while the shift reactor section aims to convert the CO products generated by the reformer section, as per Eq. (1b). The WGS reaction is exothermic, so it is favored at lower temperatures compared to the net endothermic reforming reactions. Hence, in order to convert the remaining CO into CO_2 to create more H_2, shift reactions take place at lowered temperatures. In the shift reactors, different catalysts are employed for the high-temperature and low-temperature WGS (LT-WGS) reaction. The operational conditions for these shift reactors are defined according to Chen and Chen (2020). For the high-temperature WGS (HT-WGS), an adiabatic reactor using a *RPLUG* block is chosen and the Fe–Cr commercial catalyst is used. Based on Park et al. (2009), the rate equation in Table 1 ($r_2^{HT\text{-}WGS}$) is used to simulate the HT-WGS catalytic reaction rate with the Fe–Cr commercial catalyst. For the low-temperature WGS, a second adiabatic *RPLUG* reactor block is chosen and based on Mendes et al. (2010), the rate equation in Table 1 ($r_2^{LT\text{-}WGS}$) is used to simulate the LT-WGS catalytic reaction rate with the $CuO/ZnO/Al_2O_3$ commercial catalyst. The sizing of the shift reactors was based on the criteria set fourth by Rase (1977) in

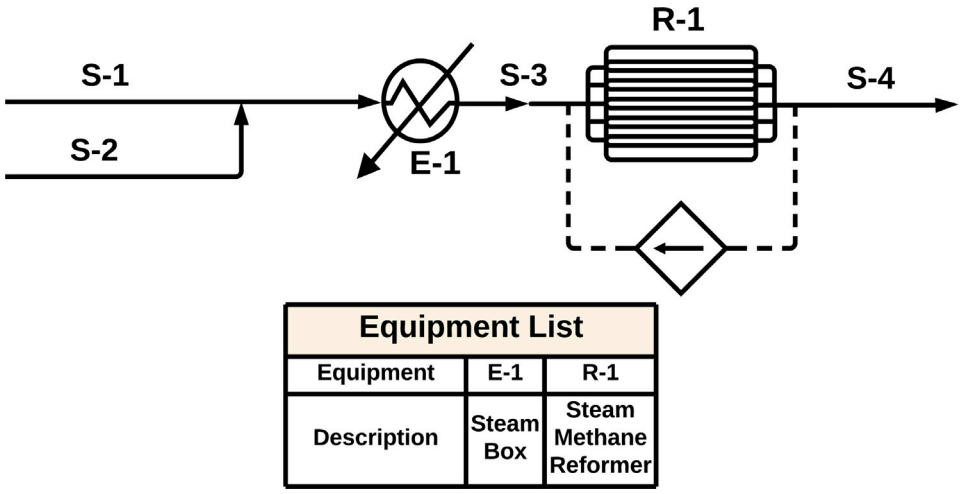

Fig. 1. Aspen Plus reformer model emulating the Joule-heated experimental setup.

Table 1
Operational parameters for industrial-scale H_2 production process simulation in Aspen V12.

Process	Description
SMR	Plug flow reactor with Ni/ZrO_2 washcoated catalyst. Operating conditions: 868–1028 °C, 16 bar Length: 4.57 m Diameter: 0.0099 m No. tubes: 774 Catalyst weight: 15 kg $r_1^{SMR} = \frac{k_1^{SMR}}{P_{H_2}^{2.5}} \frac{P_{CH_4}P_{H_2O} - P_{H_2}^3 P_{CO}/K_{eq,1}^{SMR}}{\left(1 + K_{CO}P_{CO} + K_{H_2}P_{H_2} + K_{CH_4}P_{CH_4} + K_{H_2O}P_{H_2O}/P_{H_2}\right)^2}$ $r_2^{WGS} = \frac{k_1^{WGS}}{P_{H_2}} \frac{P_{CO}P_{H_2O} - P_{H_2}P_{CO_2}/K_{eq,1}^{WGS}}{\left(1 + K_{CO}P_{CO} + K_{H_2}P_{H_2} + K_{CH_4}P_{CH_4} + K_{H_2O}P_{H_2O}/P_{H_2}\right)^2}$
HT-WGS	Plug flow fixed bed reactor contains a $Fe_2O_3/Cr_2O_3/CuO$ based catalyst. Operating conditions: 449–543 °C, 15.8 bar Packed bed length: 1.58 m Packed bed diameter: 0.79 m Catalyst weight: 500 kg $r_2^{HT\text{-}WGS} = 10^{5.854} \exp\frac{-1.11\times10^5 \pm 2.63}{RT} P_{CO}^{1.0} P_{CO_2}^{-0.36} P_{H_2}^{-0.09}\left(1 - \frac{1}{K_2}\frac{P_{CO}P_{H_2}}{P_{CO}P_{H_2O}}\right)$
LT-WGS	Plug flow fixed bed reactor contains a $Cu/ZnO/Al_2O_3$ based catalyst. Operating conditions: 251–274 °C, 15.2 bar Packed bed length: 1.42 m Packed bed diameter: 0.71 m Catalyst weight: 100 kg $r_2^{LT\text{-}WGS} = 1.329 \exp\frac{-34.983\times10^3}{RT} P_{CO}^{0.854} P_{H_2O}^{1.99} P_{H_2}^{-1.926} P_{CO_2}^{-0.573}\left(1 - \frac{1}{K_2}\frac{P_{H_2}P_{CO_2}}{P_{CO}P_{H_2O}}\right)$

their reactor design case study that suggests a 4.5 s residence time for each shift reactor and a length-to-diameter ratio of about 2:1. Per this instruction, the shift reactors' packed beds are 1.58 m and 1.42 m long with outer diameters of 0.79 m and 0.71 m for the HT-WGS reactor and the LT-WGS reactor, respectively. The residence times of the shift reactors are 4.3 s and 4.5 s for HT-WGS and LT-WGS reactors, respectively, and the effluent gas from the HT-WGS and LT-WGS section is subsequently purified. The main molecules that need to be removed from this effluent stream are steam and CO_2. Steam removal is achieved through a condenser, as steam can be liquefied at lower temperatures, and any remaining water is removed through a molecular sieve dryer. The dryer mitigates the influence of water content on the PSA unit as molecular sieve adsorption beds with zeolite 3 A can adsorb residual process water. The recent work by Gabelman (2017) indicated that the water-holding capacity of a 3 A molecular sieve zeolite is typically 20% of the weight of the sieve. In addition, Terrigeol and Trifilieff (2015) implied that the water adsorption bed is regenerated after 12–36 h of adsorption in industrial settings. In this study, two adsorption beds, each containing 675 kg of a 3 A zeolite molecular sieve, are utilized. One bed operates for 24 h to remove water from the stream. Once this bed becomes saturated with water, it undergoes regeneration, while the stream is diverted to the other bed to continue the adsorption process. The subsequent stream is sent to the PSA section for purification. The PSA simulation on Aspen Adsorption V12 is incorporated into the steady-state Aspen Plus V12 simulation with a user model block that has defined split fractions derived from the PSA simulation. The final outlet stream of the overall process contains 99% pure hydrogen. The gas stream leaving the dryer is mainly composed of H_2 and CO_2. Subsequently, CO_2 removal is accomplished via the PSA process, from which the effluent yields high-quality H_2 production with 99% purity.

3.2. Aspen plug flow reformer model comparison to experimental results

The Aspen reformer process faithfully models the experimental setup (Fig. 1), using the same dimensions, inlet flowrates for each gas (including Argon which is used as a tracer in the experimental setup), catalyst weight, and operational temperatures. The experimental setup employs two K-type thermocouples located on the reactor wall of

the inlet section and of the outlet section. Experimental temperatures were recorded from both thermocouples and used as inputs to the *RPLUG* reactor to represent the tube inlet and outlet temperatures. The experimental electrified SMR process contains a series of mass flow controllers that modulate and maintain the inlet flow streams of CH_4, H_2, and Ar (39.4/17.7/6.5 sccm). It is a common industrial practice to flow hydrogen in the inlet feed to limit the forward progression of side reactions that produce coke. For example, the reverse of the methane cracking reaction is favored at higher concentrations of H_2. All e-SMR experiments and simulations have hydrogenated inlet feeds for this reason.

Upon entering the e-SMR system, the dry gas inlet mixture with hydrogen travels through a bubbler where it is mixed with water vapor in a 3:1 S/C ratio. To generate the appropriate steam flowrate to achieve this ratio, a Watlow PI controller regulates the energy input to the heating tape that surrounds the stainless steel bubbler casing. The temperature setpoints of the gas bubbler to produce a 70% steam inlet mixture, or 119.5 sccm, are 96 °C at 1 bar and 144 °C at 5 bar. The bubbler efficiencies are known to be around 94% so the temperature setpoint is slightly higher than the theoretical setpoint. After the dry gas stream is mixed with water vapor at the desired S/C ratio, the stream is heated to 150 °C. The mixture proceeds to the reformer built from a 5.4 mm diameter and 500 mm length Goodfellows FeCrAlloy © tube where the gasses come into contact with Ni surface sites on a ZrO_2 washcoat. The Ni loading in the reformer is 158.0 mg which is also the catalyst weight used for computational modeling. The reformer effluent flows through a stainless-steel shell casing, cooled by ambient temperature water. Cooled, unreacted water vapor liquefies and collects in condenser bottles. The remaining gas product mixture flows through an automated gas chromatograph (GC), and the mixture components are quantified before venting.

To validate the Aspen Plus electrified reformer simulation model, steady-state data collection occurred at 1 bar and 5 bar system pressures over the outlet temperature range of 500 to 800 °C. A theoretical heat flux profile is provided as an input to the experimental-scale Aspen reformer model to adequately describe energy consumption and generation driven by the SMR and WGS reactions over the length of the reactor. The heat flux parameters of the Aspen plug flow reformer model were adjusted to mirror the experimental thermocouple measurements at 34.25 cm and 13.5 cm from the reactor outlet. The heat flux configurations with temperature and CH_4 conversion results are provided in Fig. 2. Specifically, the heating profiles programmed in Aspen are shown in Figs. 2(a) and 2(b). The initial heat flux consumed by the SMR reactions is higher for the first 40% of the tube length, where the endothermic reaction dominates. For the remainder of the tube length, the WGS reaction dominates, providing exothermic heat to the reformer and lessening the energy flux requirement. This behavior is the same for all reformer simulations, and the inlet heat flux requirements range from 0.662 kW/m^2 to 3.11 kW/m^2 under the different system pressures. Given additional axial temperature measurements, the programmed flux profile would gain accuracy and become increasingly linear, as seen in the e-SMR experiments conducted by Wismann et al. (2019). It is also thought that the resulting temperature profiles, seen in Figs. 2(c) and 2(d), would become increasingly linear as well. Still, the programmed heating profiles provide a good estimate of the average energy requirements over the entire length of the reactor as evidenced by the general agreement between the experimental and computational gas product molar flowrates in Figs. 3 and 4. Further, the conversion profiles at both pressures, being aligned with the position-dependent temperature measurements, reveals most methane conversion occurs in the first 50% of the reactor length, with much less conversion occurring in the second 50%. The only exception to this trend occurs for the 479.6 °C steady-state at 1 bar and the 463.3 °C steady-state at 5 bar. At lower temperatures, the conversion is lower, and thus the heat flux is more homogeneous along the length of the reactor.

Temperature control over the experimental reformer to ramp and maintain the outer wall temperature of the tube is provided in detail in Cui et al. (2024) and Çıtmacı et al. (2024a,b). Experimental results were expected to follow the conversion trends of the Aspen PFR computational model with changes in temperature and pressure. However, considering molecular dissociations into carbon atoms by CH_4 thermal decomposition (Ashik et al., 2017), the Boudouard, and CO disproportionation (Ginsburg et al., 2005) reactions at higher steady-state temperatures, larger absolute errors between Aspen-predicted and experimentally-measured CO and CO_2 flowrates were also anticipated (Fig. 5(a)). Rates of carbon formation (coking) tend to increase with temperature, and carbon formation peaked at 5 bar and 747.5 °C assuming all losses to the carbon balance, in sccm units, result from missing CH_4 that has turned into solid carbon. Experimental heat losses are documented in Fig. 5(b) which shows the average external heat loss from the reformer's outer wall into the surroundings. It is also thought that the packed bed kinetic model, adopted from Xu and Froment (1989), differs from the Ni/ZrO_2 washcoat kinetics. The over-prediction of the Aspen PFR model in Fig. 2(c) is thought to reflect the physical geometric difference between the packed bed and washcoat along with the impact of catalyst geometries on bulk mass transfer to Ni active sites. Additionally, the fraction of the total energy that is not consumed by the internal reforming reactions is reported. External heat losses range from 5.95 to 13.62 kW/m^2 and increase with the steady-state temperature of the reformer. The fractional heat losses, dependent on methane conversion, range from 90.7% to 94.4% and are minimized at 556.4 °C under 5 bar conditions. With over 90% of energy losses to ambient surroundings, this novel process stands to gain the most percentage points in energy conversion efficiency from improvements to the thermal insulation layer encapsulating the reformer. Root-mean-squared-error (RMSE) values were used to establish the performance of the 1 bar and 5 bar Aspen PFR steady-state simulations. At 1 bar, the errors for CH_4, H_2, CO, and CO_2 were 4.26, 22.97, 5.38, and 5.41, respectively. It is thought that the hydrogen error was exacerbated by lower mass transfer to Ni surface sites on the washcoat at lower pressures or by the inhibition of active catalytic sites due to carbon formation. It may also be possible that the larger error in H_2 measurements is a byproduct of the larger magnitude of the hydrogen flowrate in comparison to the other gas product species. Further, GC measurement errors range from 1%–5% and contribute to the model error as well. The RMSE values for the 5 bar steady-state measurements and CH_4, H_2, CO, and CO_2 predictions were 3.34, 9.62, 7.12, and 2.48, respectively. Most notably, the gas product trends align with the Aspen models, providing an experimental validation for high-pressure process intensification.

Reformer conversion efficiencies were calculated using Eq. (2):

$$eff_{\text{Energy}} = \frac{(\dot{n}_{H_{2,\text{Out}}} - \dot{n}_{H_{2,\text{In}}}) \times HHV_{H_2}}{\dot{n}_{CH_{4,\text{In}}} \times HHV_{CH_4} + Average\ Power\ Input} \times 100\% \quad (2)$$

where the reformer energy conversion efficiency is equal to the molar flowrate of hydrogen produced times the higher heating value (HHV) of hydrogen gas divided by the quantity that multiplies the molar flowrate of inlet methane with its HHV and adds the average power input from the DC power supply. This calculation is formulated as such to provide a ratio of the output energy stored in the chemical bonds of the H_2 target product to the input energy in the form of resistance heating and chemical energy stored in CH_4 molecules. The optimal energy conversion efficiencies for the 1 bar and 5 bar experiments were achieved at the 663.6 °C and 659.4 °C steady-state temperatures, which are calculated using an arithmetic average of the top and bottom thermocouple values. Fig. 6 shows a 20.2% energy conversion efficiency at 1 bar which increases to 22.7% around the same temperature at 5 bar. In the Aspen simulation, optimal energy conversion efficiencies occur at the 749.8 °C and 747.5 °C steady-state temperatures. The energy efficiency of the 1 bar simulation at the aforementioned temperature is 83.2% which exceeds the optimal efficiency of the 5 bar simulation by 2.0%.

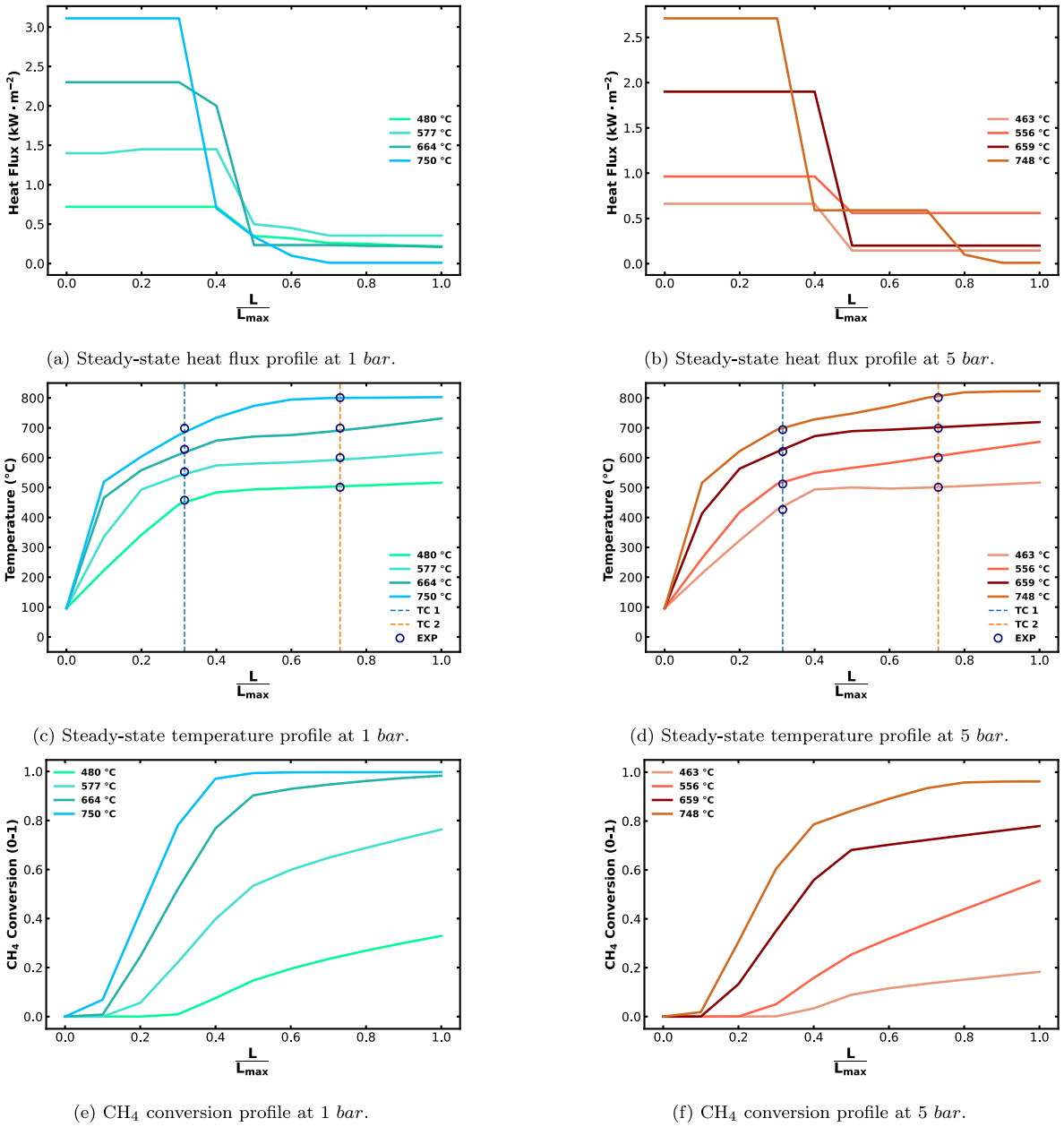

(a) Steady-state heat flux profile at 1 *bar*.

(b) Steady-state heat flux profile at 5 *bar*.

(c) Steady-state temperature profile at 1 *bar*.

(d) Steady-state temperature profile at 5 *bar*.

(e) CH_4 conversion profile at 1 *bar*.

(f) CH_4 conversion profile at 5 *bar*.

Fig. 2. Aspen plug flow reforming reactor simulation; heat flux configuration with temperature and conversion results as a function of the reformer length.

Considering the Aspen model is not equipped to account for external heat losses to the surroundings, the simulation energy efficiencies are about four times that of the experiments at either system pressure. The average heat loss to the surrounding environment is provided in Fig. 5(b). In the future, experimental energy losses can be minimized by providing better thermal insulation to the reformer tube and to the upstream and downstream pipelines. It must also be added that some of the power input to the experimental system goes into heating the insulation layers and surrounding metals. As a consequence, there is a large inertial mass that is heated as the experimental bench setup is operated at higher temperatures. These heat losses will be minimized in industrial electrified reformers.

3.3. Scaling up of the experimental SMR process: Design parameters

In literature, e-SMR experiments have been conducted using one hourly space velocity while their accompanying computational models use an entirely different hourly space velocity which has transport implications for heterogeneous catalysis in gas-phase reactors. Though changing space velocities may not induce mass transfer limitations of bulk CH_4 to a packed bed catalyst in a flow reactor, changes to the hourly inlet flowrates to a reformer volume with a washcoated catalyst can reduce the mass transfer of bulk CH_4 to embedded Ni catalyst active sites. Unlike the packed bed arrangement of a catalyst, a washcoat catalyst is placed on the inner wall of a tube, and the reactants must travel in the radial direction of the tube towards the Ni surface sites. Therefore, it is possible that some of the reactant in the center of the tubes may never reach these surface sites, depending on the bulk mass transfer distribution in the tube. To maintain the axial convection, bulk mass transfer, and conversion of reactants in the experimental system, thus ensuring the viability of the proposed (Xu and Froment, 1989) kinetic model for the Ni/ZrO_2 washcoat at industrial scales, the design criteria for the industrial reformer was set by the second Damkhöler number (Da_{II}). The second Damkhöler number is a dimensionless parameter that describes kinetic and external mass transfer rates in a chemical reaction control volume. Higher values for

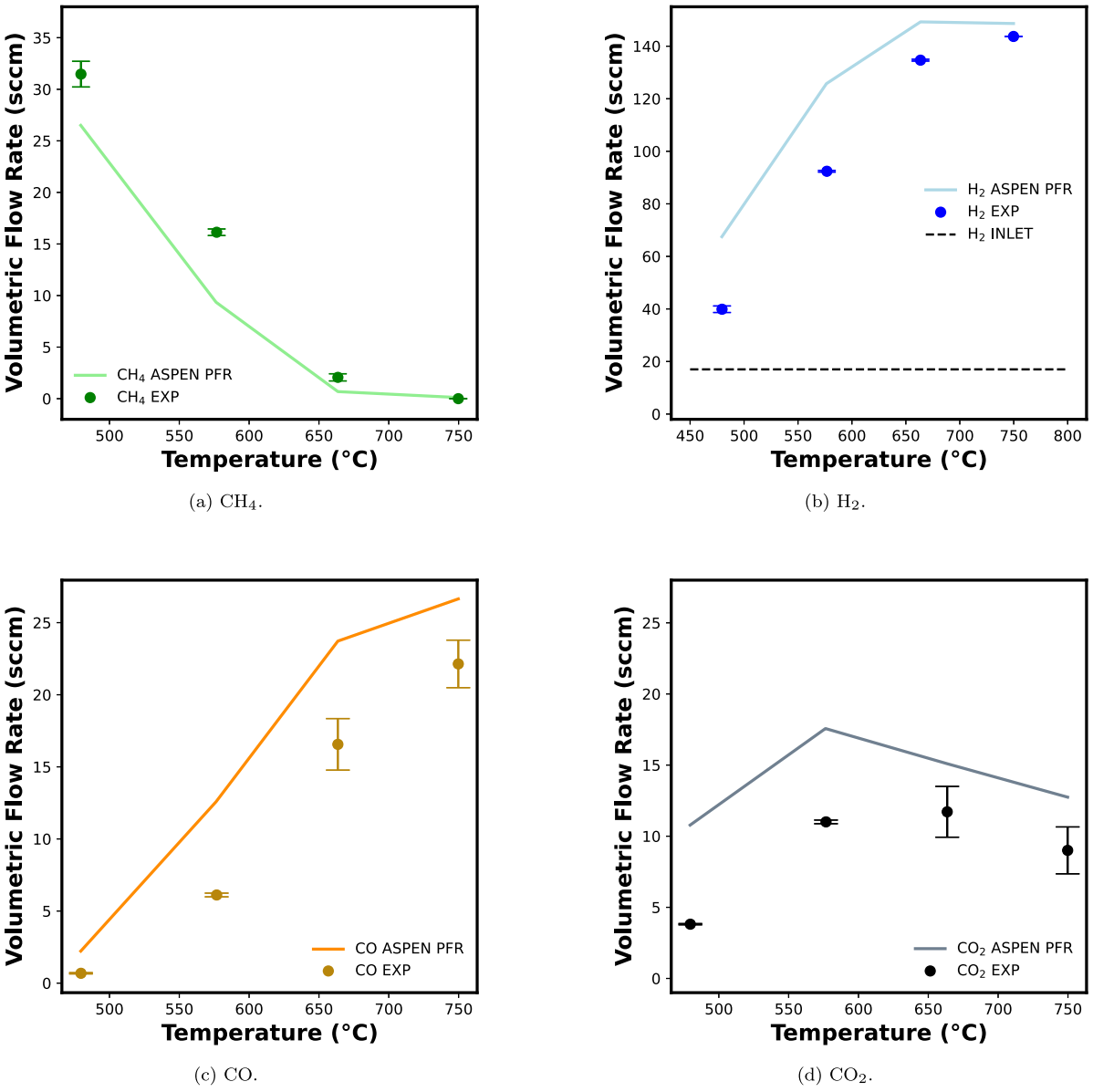

(a) CH_4. (b) H_2.

(c) CO. (d) CO_2.

Fig. 3. Joule-heated experimental gas product stream comparison to the Aspen Plus SMR reactor model at 1 bar. The error bars represent the standard deviations of steady-state GC measurements.

Da_{II} signify external mass transfer inhibition to the catalyst surface, whereas lower values for Da_{II} describe kinetically-limited complexes with few active catalyst sites. Given a system where both external mass transport to a catalytic washcoat and the residence time for the reactants must be considered, as is true for the e-SMR, Da_{II} provides an observable effective reaction rate by establishing the ratio between the characteristic mass transfer and reaction times. The equation for Da_{II} assuming CH_4 is the limiting reactant and there is no internal mass transfer of CH_4 through the catalytic washcoat is:

$$Da_{II} = \frac{t_m}{t_r} = \frac{r_{net}}{k_m \cdot a \cdot C_{CH_4,inlet}} \tag{3}$$

where the second Damkhöler number equals the ratio of the characteristic mass transfer time to the characteristic reaction time. For an SMR process, the aforementioned ratio is equivalent to the net SMR reaction rate divided by the product of the mass transfer coefficient, the specific surface area of the washcoat catalyst, and the inlet concentration of CH_4.

The mass transfer coefficient describing the transport of bulk reactant to Ni surface sites on the catalytic wall driven by the diffusion, advection, and mixing of CH_4 towards the washcoat surface can be calculated using the following relation:

$$k_m = \frac{Sh_\infty D_m}{d_h} \tag{4}$$

where the mass transfer coefficient for a single tube is equal to the asymptotic Sherwood number times the mass diffusivity of CH_4 in the gas inlet mixture divided by the hydraulic diameter of the reformer tube ($d_h = d_t$ for circular tubes). The Sherwood number characterizes the ratio of convective mass transport to diffusional mass transfer. For larger Sherwood numbers, the concentration gradient in the radial direction from the reformer tube center to the catalytic wall is large when the mass transfer coefficient of methane from the bulk to the solid Ni/ZrO_2 phase is large and the velocity and concentration boundary layers are thin; consequently, CH_4 can reach the catalyst wall surface quickly and react. Limited by a larger boundary layer thickness and smaller CH_4 concentration gradient, the opposite is true for lower Sherwood numbers for which the transfer of bulk CH_4 molecules to the solid catalyst is less effective. The minimum length at which the boundary layer thickness becomes constant in the reformer corresponds to the

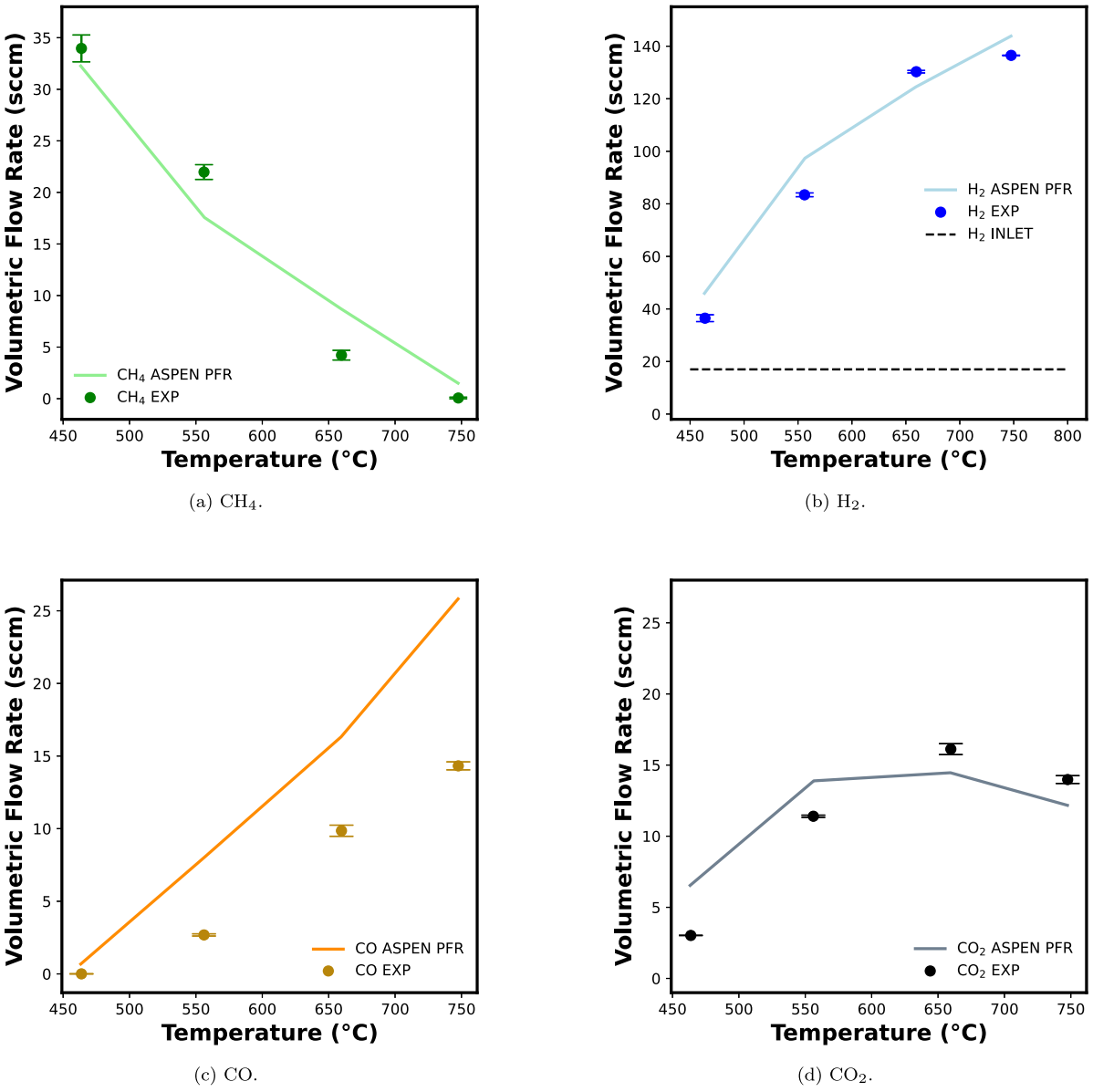

(a) CH_4. (b) H_2.

(c) CO. (d) CO_2.

Fig. 4. Joule-heated experimental gas product stream comparison to the Aspen Plus reformer model at 5 bar. The error bars represent the standard deviations of steady-state GC measurements.

asymptotic Sherwood number, marking the end of the hydrodynamic entrance and the beginning of a fully developed flow regime. The length of the designed reactor tube should be sufficiently large to ensure the asymptotic Sherwood number is reasonable, according to the following condition:

$$L_t \geq 0.05 \cdot Re \cdot Sc \cdot d_h \tag{5}$$

To determine Da_{II} for the single-tube reformer, the mass transfer coefficient for CH_4 transport was calculated from Eq. (4) using the inlet diffusivity of CH_4 and water vapor in the bulk mixture that flows through the reformer. A characteristic mass transfer time on the order of 10^{-2} s is proposed by this calculation method. The characteristic reaction time, using the initial reaction rate, is on the order of 10^{-1} s, and the value of Da_{II} for the experimental reformer is 0.14. A Da_{II} value that is close to 1 signifies a balanced interplay between the supply of CH_4 to the Ni/ZrO_2 wall and the SMR conversion chemical conversion rate, however, a Da_{II} around 0.1 implies the experimental setup is kinetically-controlled. The large-scale reactor diameter is therefore designed to ensure the same value for Da_{II} as the experimental reformer.

A key difference between a lab-scale and industrial SMR process is the number of tubes, or reactor coils, that are used to distribute the flow of reactants through the total reactor volume. Increasing the total number of tubes in a reformer will alter the velocity profile of bulk reactants and change the thickness of the CH_4 concentration boundary layer. To address the physical changes to the reformer unit induced by geometric modifications, characteristic mass transfer analysis in a multitubular system must be described using a global mass transfer coefficient. According to Kashid et al. (2014), the global mass transfer coefficient of bulk reactant to Ni surface sites on the catalytic walls of a multitubular industrial reformer can be represented by the following relations:

$$k_G = \frac{Sh''_\infty D_m}{d_h} \tag{6a}$$

$$Sh''_\infty = \frac{1}{Sh'_\infty} + \frac{Da_{II}}{Da_{II} + 1.979}\left[\frac{1}{Sh_\infty} - \frac{1}{Sh'_\infty}\right] \tag{6b}$$

where the global mass transfer coefficient for a multitube reformer is equal to the product of the multitube asymptotic Sherwood number

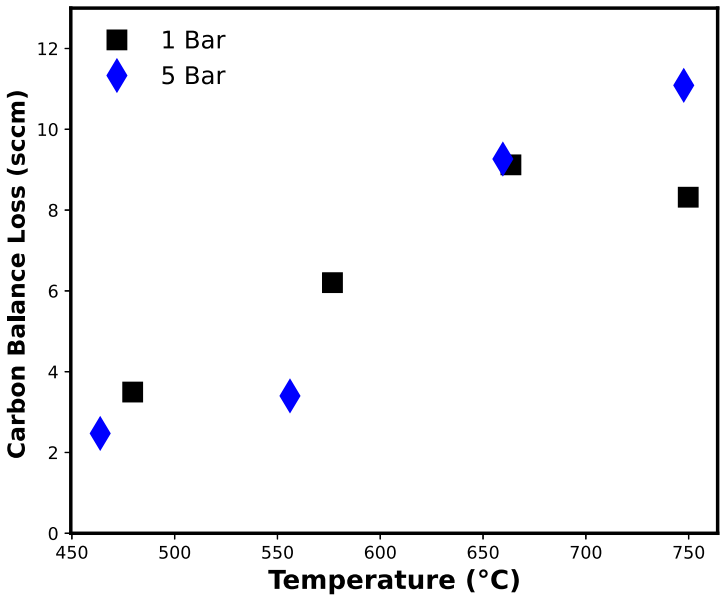

(a) Experimental carbon balance error introduced by varying levels of solid carbon formation.

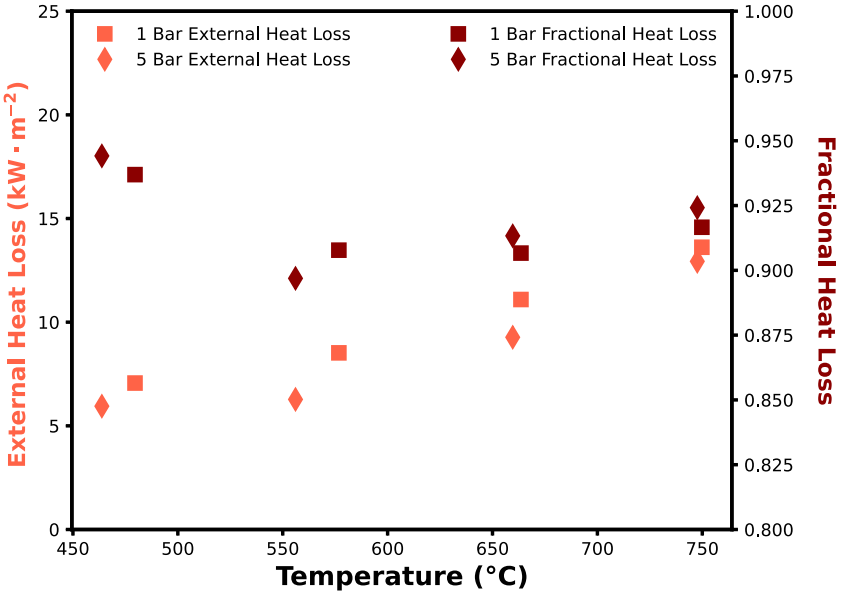

(b) Experimental external heat flux to the surroundings (heat losses that are not kinetically consumed).

Fig. 5. Experimental heat energy and carbon balance losses at 1 bar and 5 bar for 463 to 750 °C steady-state temperatures.

for a chemical reaction (Sh''_{∞}) and the mass diffusivity of CH_4 in the gas inlet mixture divided by the hydraulic diameter of a single tube. To obtain Sh''_{∞}, Eq. (6b) is used where the values of Sh_{∞} and Sh'_{∞}, the asymptotic Sherwood number for a zero-order reaction, are 3.66 and 4.36, respectively (Kashid et al., 2014). The only unknown in Eq. (6) is d_t, which was solved for after determining a characteristic reaction times for an electric reformer with 15 kg of catalyst at different pressures and temperatures. For an industrial flow rate of pure CH_4, the tube diameter that maintained the experimental Da_{II} was 9.88 mm. Once the tube diameter was specified, Bodenstein numbers (Bo) elucidated the appropriate tube length to allow for a fully-developed flow, a linear velocity between 0.5–1.5 m/s, and a reasonable number of tubes (on the order of 10^2). The Bodenstein number is yet another dimensionless parameter which compares the axial convective transport rate in a flow reactor to its diffusion transport rate (Kashid et al., 2014). Specifically, the Bo number represents the ratio between axial dispersion time and the average residence time of reactants. A small Bo value indicates a shorter dispersion time, high rates of diffusion compared to axial convection, and a complete backmixing of reactants and products in the reactor as seen in continuously stirred tank reactors. Alternatively, larger Bo values are calculated for flow reactors that experience negligible dispersion and little backmixing. Plug flow behavior is usually represented by a Bo number between 100 to 1000 (Kashid et al., 2014). Using Eq. (7a), the Bo number for a flow system can be

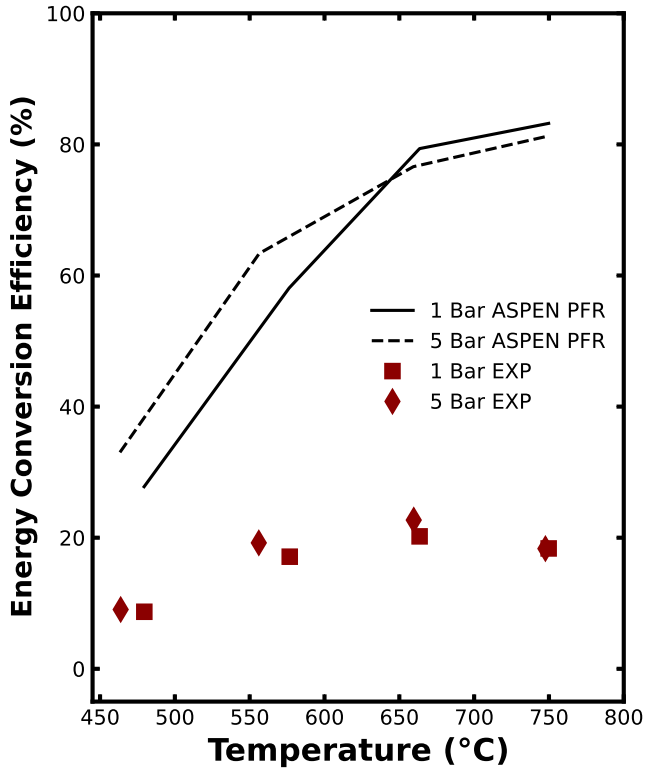

Fig. 6. Aspen Plus *RPLUG* electric reformer model (Fig. 1) and experimental energy conversion efficiencies (Eq. (2)) as a function of temperature and pressure.

determined as a function of the linear velocity of fluid flow, the length of the reactor, and the axial dispersion coefficient.

$$Bo = \frac{uL_t}{D_{ax}} \tag{7a}$$

where Bo is equal to the product of the linear velocity of fluid flow and the length of the reactor divided by the axial dispersion coefficient. Further, Eq. (7b) provides the following relation to evaluate the axial dispersion coefficient:

$$D_{ax} = D_m + \chi \frac{u^2 d_t^2}{D_m}, \quad \chi = \frac{1}{192} \ [for\ circular\ tubes] \tag{7b}$$

where the axial dispersion coefficient for the reactant mixture is equal to the diffusivity of a gas specie in a mixture plus the product of the characteristic geometric factor for the control volume with the square of linear velocity of the fluid and the square of the tube diameter divided by the diffusivity of the gas specie. Using multiples of the length-to-diameter (L_t/D_t) ratio from the Goodfellows' tube dimensions, a sensitivity analysis, shown in Fig. 7, was conducted for different reformer lengths and Bo numbers. The optimal set of dimensions that obeyed the linear velocity and tube quantity constraints was a reformer with 774 tubes with a 9.9 mm inner diameter (ID) and 4.57 m length. Assuming the average kinematic viscosity over the length of a reforming tube adequately describes its flow regime, the flow in each of the tubes at elevated temperatures remains laminar (Reynold's number around 1000) and each tube's hydrodynamic entrance zone is 0.43 m. It is important to note that this design is not unique and a reformation system consisting of 552 tubes with a linear velocity of 2.1 m/s and Reynold's number of 1409 is another potential configuration. More generally, the sensitivity analysis shows that when Bo equals 10, linear velocities around 10^1 m/s occur. As a consequence, fewer tubes are needed to distribute the total volumetric flow rate of the reacting species. At the other extreme, when Bo is equal to 1000, an ideal plug flow behavior is reached at lower linear velocities in the reformer tubes because the total volumetric flow rate is distributed across a greater number of tubes.

3.4. SMR flowsheet overview

The scaled-up version of the SMR simulation, referred to here and throughout the rest of this study, incorporates essential unit operations and adjusts the process inlet parameters according to prior experimental findings. The configuration of the reactors is mentioned in Table 1. At the beginning of the flowsheet, pressurizing CH_4 and H_2O is essential for operating at industrial scales because of equipment sizing constraints. Increasing the pressure also helps to maintain the GHSV of 1000 h^{-1} from the experimental setup. The methane stream undergoes pressurization through a multistage compressor, which consists of 3 stages with an equal pressure ratio of 2.51 and intercoolers that are specified such that the ratio of outlet temperatures to inlet temperatures at every stage is 0.85. The simulation gives better energy conversion and total system efficiencies at lower pressures; however, this would lead to impractical reformer tube diameters for the same space velocity. The multistage compressor is followed by the mixing of CH_4 with the preheated steam using a mixer. The water stream is at a temperature of 201 °C which is essential for maintaining a S/C ratio of 3 at the operating pressure. This mixed stream is fed into the steam methane reformer and the outlet temperature for the reformer varies from 868 to 1028 °C depending on the chosen heat flux values. The compressed, wet reactant stream undergoes the steam methane reforming reaction (Eq. (1a)) and (Eq. (1b)) in the presence of the Ni/ZrO_2 catalyst, following the kinetics described by Xu and Froment (1989). Subsequently, the stream is cooled and is fed into the high-temperature water gas shift reactor, HT-WGS as seen in Fig. 8. The stream undergoes catalytic reaction at 449 °C with the reaction rate ($r_2^{\text{HT-WGS}}$ in Table 1). Afterward, the cooled product stream of the HT-WGS reactor feeds into the low-temperature water gas shift reactor and undergoes the water gas shift reaction at 252 °C with reaction rate ($r_2^{\text{LT-WGS}}$ in Table 1). Thereafter, the product stream is brought to 25 °C and then flashed. The condensed water is removed through the bottoms and the vapor containing hydrogen is sent to the molecular sieve to eliminate the remaining water as seen in Fig. 9. Finally, the vapor-containing stream is sent all the way downstream to PSA section for the recovery of high-purity hydrogen product.

4. Pressure swing adsorption simulation with Aspen adsorption

A continuous PSA process requires at least two columns packed with an adsorbent material, which selectively adsorbs gas mixture impurities, while the separation target gas (such as H_2) passes through. During this process, a gas mixture is pushed through a packed adsorbent bed using high pressures in the adsorption column. After some time of adsorption through either bed, the bed saturates and the tank must be depressurized to release the purified target product. This causes an inherently dynamic process, where the bed is pressurized until the saturation of the bed, and is depressurized until the bed can be used again. When one is pressurized, the other one is depressurized and vice versa. As a result, the gas mixture is continuously separated. A process diagram of the Aspen Adsorption simulator is shown in Fig. 10. The columns are designed with respect to industrial pressure scales, cycle times, and gas flow velocities, which were inspired by available patents for the process. Based on these parameters, a suitable column diameter and bed length were selected and are shown in Table 4. The inlet gas mixture to PSA columns is composed of different compositions, depending on the steam methane reforming process. An extensive outlet temperature range of the reformer is simulated to generate gas composition results, and the gas composition range is used to design the PSA process.

The simplified Skarstrom cycle is considered in the PSA simulation process, of which the steps are shown in Fig. 11 (Skarstrom, 1963).

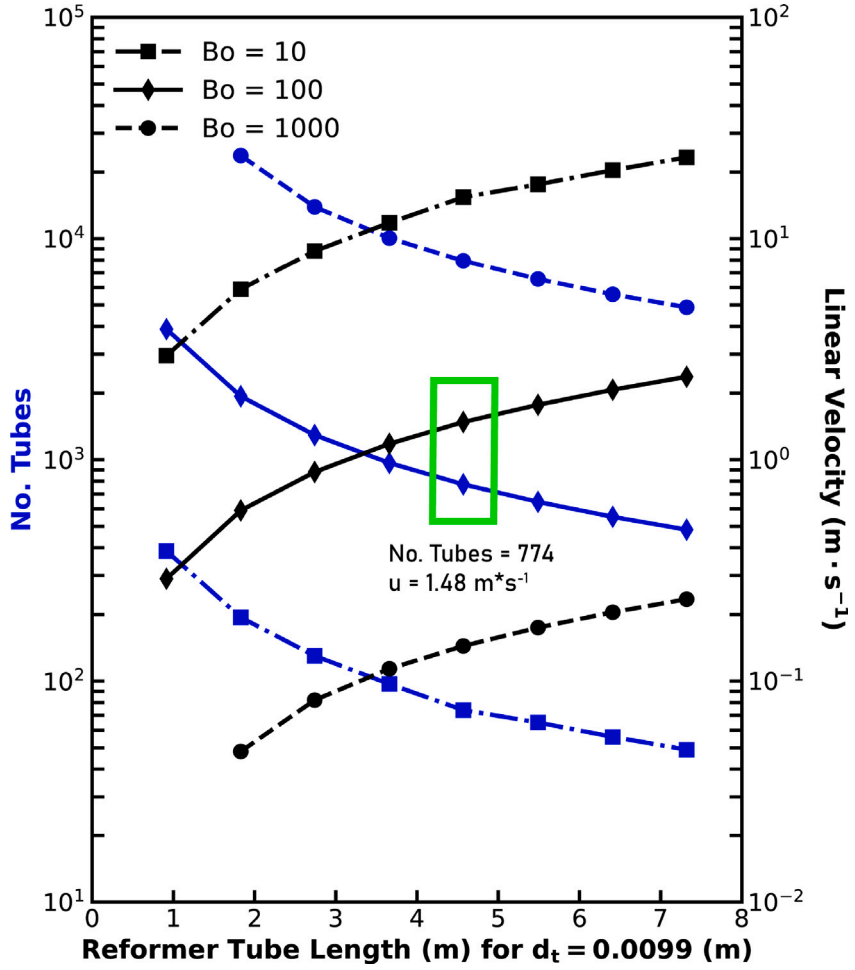

Fig. 7. Reformer sizing for different Bodenstein numbers given a fixed tube diameter of 0.099 m as determined by Eq. (7a). Blue lines display the number of tubes (coils) and black lines display the linear velocities of gas flows in the industrial-scaled reformer as a function of tube length and Bo (inlet molar flowrate = 37 mol/s). (For interpretation of the references to color in this figure legend, the reader is referred to the web version of this article.)

The first step in the cycle is to pressurize bed T-2a by feeding in a high pressure gas mixture with the goal of separating H_2 (Fig. 11(a)). Meanwhile, a portion (usually around 15%) of the gases in bed T-2a flows into bed T-2b to depressurize and regenerate the bed. Once the pressure in the beds reaches the desired value, the process proceeds to the next step. In the second step (Fig. 11(b)), the valve V-4 shown in Fig. 10 is opened to allow high purity hydrogen to exit the bed as product flow. As the adsorption step progresses, an increasing amount of adsorbent sites become saturated by the feed gases, resulting in a decreased separation ability of the bed. Therefore, we are using bed T-2b for the adsorption process by step 3 (Fig. 11(c)) and step 4 (Fig. 11(d)), while bed T-2a is regenerated.

4.1. Adsorption model

The simulation relies on principles of mass, momentum, and energy conservation, as well as adsorption isotherms. Aspen Adsorption incorporates a mathematical dynamic model due to the time-varying nature of the PSA process based on the one spatial dimension assumption from Wood et al. (2018) to facilitate these aspects. For mass transfer, a plug flow assumption without diffusion is utilized with convection, as described dynamically by Eq. (8).

Mass Transfer Conservation Equation: $$\frac{\partial C_i}{\partial t} + \rho_p \frac{1-\epsilon_i}{\epsilon_i}\frac{\partial n_i}{\partial t} + v_g \frac{\partial C_i}{\partial z} = 0 \quad (8)$$

The adsorption kinetics adhere to the linear driving force (LDF) model, characterized by a constant mass transfer coefficient, as indicated in Eq. (9).

Linear Driving Forces: $$\frac{\partial n_i}{\partial t} = MTC_i(n_i^* - n_i) \quad (9)$$

The momentum balance considers a pressure drop along the adsorption bed by using the Ergun equation, as described in Eq. (10) below:

Ergun Equation: $$\frac{\partial P}{\partial z} = -\frac{150(1-\epsilon_i)^2}{d_p^2 \epsilon_i^3}\mu v_g + 1.75\rho_g \frac{1-\epsilon_i}{d_p \epsilon_i^3} v_g^2 \quad (10)$$

Equilibrium adsorption is depicted using the extended Langmuir 3 model (Eq. (11)), an integrated feature of Aspen adsorption.

Extended Langmuir 3 Isotherm: $$n_i^* = \frac{(IP_{1i} + IP_{2i}T_s)(IP_{3i}e^{IP_{4i}/T_s})Py_i}{1 + \Sigma(IP_{3i}e^{IP_{4i}/T_s}Py_i)} \quad (11)$$

4.2. PSA simulation parameters

The industrial PSA unit capacities range from a few hundred N m^3/h to more than 400,000 N m^3/h according to Linde-Engineering (2024). In the PSA study, a 43 mol/s gas mixture with varying mole fractions (Table 2) is fed to the adsorption bed, assuming that a small-to-medium scale manufacturing facility produces the specified mixture mole fractions after the shift reactors. The exact feed mole fraction to the PSA is obtained from the Aspen Plus simulation. However, it is also important

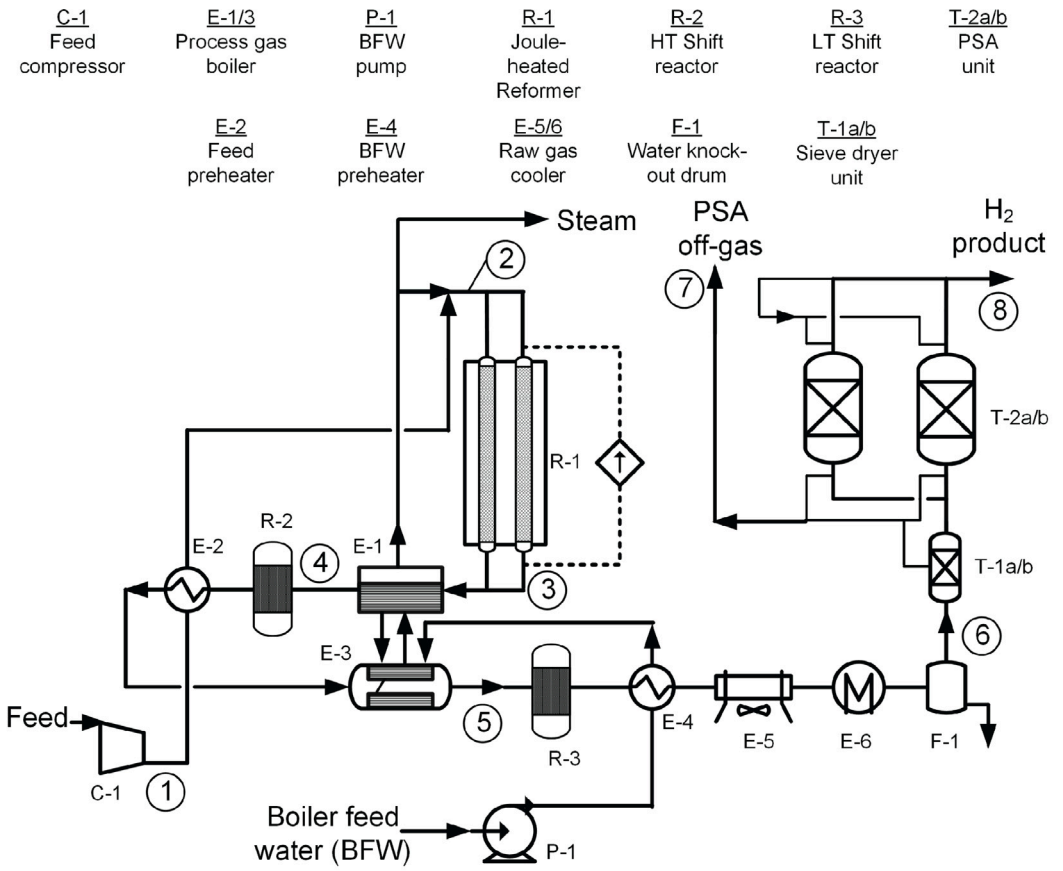

Stream No.	1	2	3	4	5	6	7	8
Mol, %	Feed	Reformer inlet	Reformer outlet	HT Shift reactor inlet	LT Shift reactor inlet	PSA unit inlet	Off-gas fuel	H_2 product
H_2	30.7	9.9	56.0	56.0	64.3	80.8	29.0	99.4
CO	0.0	0.0	11.6	11.6	3.3	1.2	3.7	0.4
CO_2	0.0	0.0	3.6	3.6	11.9	17.2	64.5	0.2
CH_4	69.3	22.4	0.4	0.4	0.4	0.5	1.9	0.0
H_2O	0.0	67.7	28.4	28.4	20.1	0.2	0.9	0.0
Flowrate, m^3 (STP)/h	974	3014	4327	4327	4327	3565	941	2623
Mass flowrate, kg/h	503	2121	2121	2121	2121	1516	1263	253
Temperature, °C	25	260	978	507	252	25	14	29
Pressure, kPa	800	1700	1600	1580	1520	1380	250	1380

Fig. 8. Optimized flowsheet of the overall SMR process comprised of an electric reformer, two WGS reactors, heat integration, raw gas cooling and drying units, and pressure swing adsorption. Comprehensive process flow diagrams for the Drying and PSA blocks are provided in Figs. 9 and 10, respectively. This process also generates 363 kg/h of saturated steam (204.5 °C and 1.7 MPa).

to note that the capacity can be increased by scaling the proposed design and employing more PSA columns in parallel. Moreover, given that the product stream before the PSA unit is primarily comprised of H_2 and CO_2 with lower concentrations of CO at high methane conversion temperatures, activated carbon is the favorable choice for an adsorbent for better separation. On the other hand, CO_2 has a large permanent quadrupole moment, therefore, it is very strongly and selectively adsorbed on a zeolite (an alternative adsorbent choice). However, it is difficult to desorb CO_2 from a zeolite adsorbent during the operation of the PSA process. In Sircar and Golden (2000), the isothermal desorption characteristics of CO_2 from activated carbon and 5 A zeolite were compared. This study demonstrated that a smaller purge stream is required to efficiently desorb CO_2 from activated carbon than from the 5 A zeolite. This indicates that despite activated carbon having moderate CO_2 capacities and selectivities compared to the zeolite, its ease of desorption makes the activated carbon a preferred adsorbent for CO_2 removal. Model parameters of the simulated adsorbent, shown in Tables 3 and 4 are taken from Ahn et al. (2001); Langmuir parameters and the LDF coefficient in Table 5 are taken from Ahn et al. (2012).

Table 2
Aspen Adsorption PSA simulation feed stream mole fractions for 7 distinct SMR outlet compositions.

No.	CH_4	CO	CO_2	H_2
1	0.19	6.63×10^{-4}	0.11	0.7
2	0.16	8.42×10^{-4}	0.12	0.72
3	0.13	1.06×10^{-3}	0.13	0.74
4	0.10	1.31×10^{-3}	0.14	0.76
5	0.06	1.70×10^{-3}	0.15	0.78
6	0.03	2.62×10^{-3}	0.162	0.81
7	4.37×10^{-3}	3.70×10^{-3}	0.17	0.82

In order to run the simulation with a specific feed flowrate, it is necessary to have the appropriate valve capacity (C_v) values, which control flowrates through adjusting valve parameters. Given that the

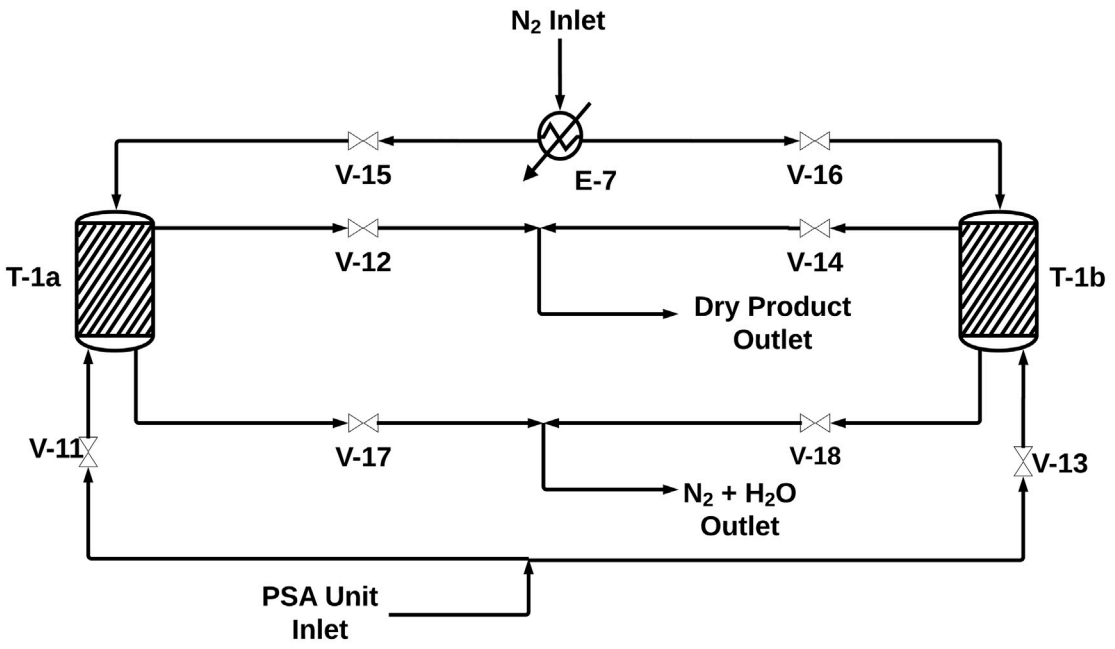

Equipment List											
Equipment	T-1a	T-1b	V-11	V-12	V-13	V-14	V-15	V-16	V-17	V-18	E-7
Description	Molecular Sieve Dryer 1	Molecular Sieve Dryer 2	Feed Valve for Dryer 1	Product Valve for Dryer 1	Feed Valve for Dryer 2	Product Valve for Dryer 2	Purge Inlet Valve for Dryer 1	Purge Inlet Valve for Dryer 2	Purge Outlet Valve for Dryer 1	Purge Outlet Valve for Dryer 2	Heater for Purge

Fig. 9. Molecular sieve dryer process flow diagram.

Table 3
Activated carbon parameters.

Average pellet radius, R_p [cm]	0.115
Pellet density, ρ_p [g/cm^3]	0.85
Bulk density, ρ_b [g/cm^3]	0.482
Bed porosity, ϵ_b	0.433

Table 4
Adsorption bed parameters.

Length, L [m]	2.3
Bed diameter, D [m]	0.5
Adsorption time [s]	280
Feed flowrate [mol/s]	43

Table 5
Langmuir parameters for activated carbon used in the Aspen Adsorption PSA model.

Component	MTC	IP_1	IP_2	IP_3	IP_4
CH_4	0.195	2.386×10^{-2}	-5.620×10^{-5}	3.478×10^{-3}	1159
CO	0.150	3.385×10^{-2}	-9.072×10^{-5}	2.311×10^{-4}	1751
CO_2	0.036	2.879×10^{-2}	-7.000×10^{-5}	1.000×10^{-2}	1030
H_2	0.700	1.693×10^{-2}	-2.100×10^{-5}	6.248×10^{-5}	1229

PSA simulation is a dynamic process, attempting to run the simulation with unsuitable C_v values often results in lack of convergence of the simulation. To address this issue, developed code tested a range of flowrate values to determine the appropriate C_v values for various pressures using mass balances.

In the simulation, an initial bed state is assumed when the adsorption bed is entirely filled with feed gas. This implies that the initial condition for the mole fractions in the adsorption bed is as shown in Table 2. Hence, conducting the simulation for approximately 2000 s is crucial to ensure that the unit attains a stable product flowrate and composition. Furthermore, to calculate the recovery and purity of H_2 in the product stream, trapezoidal integration is performed on the total flowrate and H_2 flowrate within the feed, product, and waste streams. This method allows determining the total amount of H_2 being produced by calculating the area under the flowrate curves and provides averages for steady-state production estimations of the dynamic PSA process. The aim of pressure swing adsorption in this work is to get 99% hydrogen purity in the product stream. Fig. 12 illustrates the relationship between the required separation pressure and the feed hydrogen mole fraction, ranging from 69% to 83%. This figure also demonstrates that as the proportion of hydrogen in the feed decreases, higher pressures are necessary to achieve a 99% purity of H_2 in the product gas mixture.

4.3. PSA simulation results

PSA is a dynamic process that evolves over time (Fig. 13) making it challenging to assess the performance of the unit solely based on data within 2000 s. Therefore, commonly used metrics, such as purity and recovery, are used to evaluate the effectiveness of this separation process. Additionally, integrating the PSA and steam methane reforming simulations poses a challenge due to the steady-state nature of the simulation in Aspen Plus. Employing regression analysis on the PSA variables helps to address this inherent limitation in steady-state simulations and also enhances the total efficiency of the overall plant simulation process. Fig. 14(a) depicts the linear regression analysis illustrating the relationship between the H_2 mole fraction in the feed and the requisite pressure for achieving 99% H_2 purity in the product flow. The results demonstrate a decrease in the required pressure for the product gas mixture separation with an increasing amount of H_2 in the feed flow. The R^2 value of this linear regression model is

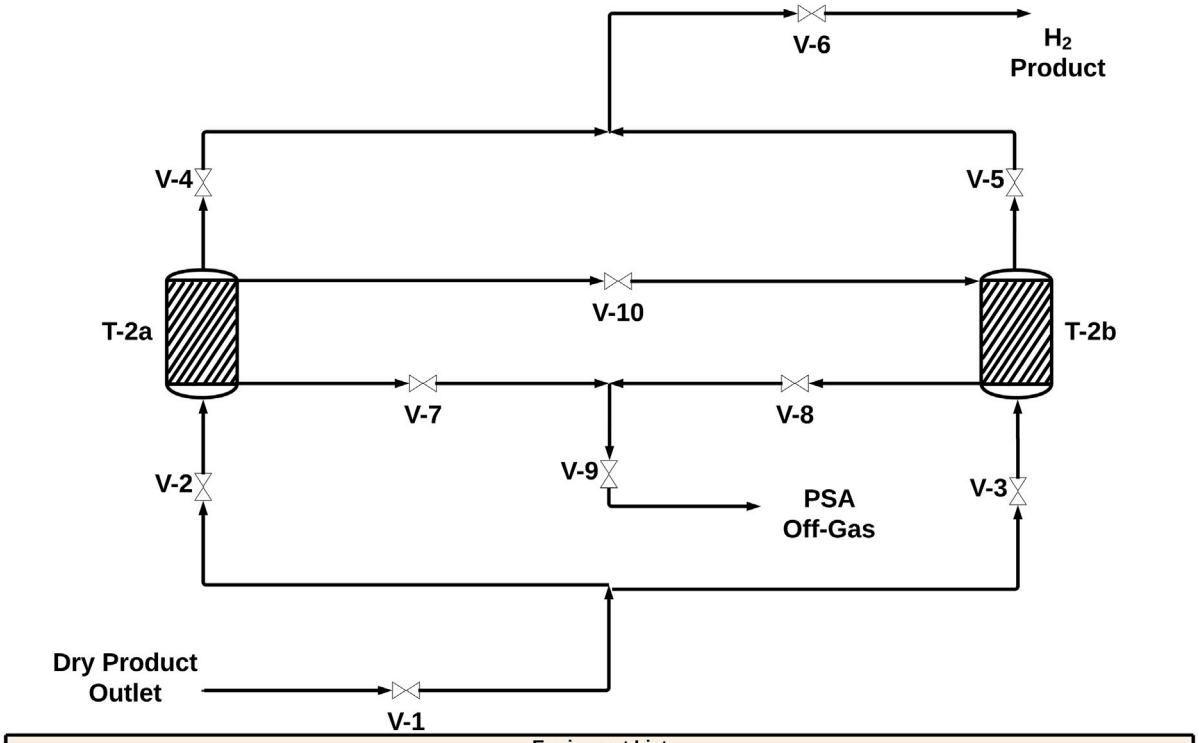

Equipment List

Equipment	T-2a	T-2b	V-1	V-2	V-3	V-4	V-5	V-6	V-7	V-8	V-9	V-10
Description	Adsorption Bed 1	Adsorption Bed 2	Overall Feed Valve	Feed Valve for Bed 1	Feed Valve for Bed 2	Product Valve for Bed 1	Product Valve for Bed 2	Overall Product Valve	Waste Valve for Bed 1	Waste Valve for Bed 2	Overall Waste Valve	Purge Valve

Fig. 10. Pressure swing adsorption process flow diagram.

0.996, indicating the adequacy of linear regression for this purpose. Fig. 14(b) presents the linear regression analysis illustrating the relationship between the requisite pressure for achieving 99% H_2 purity in the H_2 product flow and the corresponding hydrogen recovery in the H_2 product flow at that specific pressure. The analysis also indicates that for varying feed mole fractions, the H_2 recovery remains approximately 90%. In the Aspen Plus industrial-scale steam methane reforming process, the hydrogen mole fraction of the feed to the PSA system is obtained from Stream 6 (Fig. 8). By performing a regression analysis of the H_2 mole fraction and the requisite pressure needed to achieve 99% H_2 purity in the product flow, the necessary pressure for the H_2 product stream is determined. Subsequently, correlating the required pressure for separation with the H_2 product recovery through regression analysis provides insight into the efficiency of this process and is a useful tool for selecting the appropriate pressure given the desired hydrogen purity level.

5. Flowsheet optimization

5.1. Heat integration

The optimization of the flowsheet consisted of two parts. The first part included replacing the heaters and coolers with a dedicated network of heat exchangers to perform heat integration and minimize the potential of any lost duty through heat recovery. Since the outlet temperature of the reformer is significantly high, it can be used to create the pressurized steam feed. Similarly, a network of heat exchangers lowers the temperature of the reformer effluent before being sent to the shift reactors. The model fidelity of the exchangers in the Aspen Plus simulation is set to "Shortcut" and they are maintained at a hot/cold minimum approach of 50 °C with the flow direction set to countercurrent. Four heat exchangers and two coolers lower the temperature of the process gas from 978 to 25 °C. The total recovered duty from the heat integration network is 1.6 MW, excluding a utility loss of 0.7 MW. Through this method, a significant portion of the heat is recovered and utilized for steam generation.

5.2. Parametric study: Electrified SMR process

The second part of optimization involved making minor adjustments to the geometries of the units and H_2 production rates to achieve a flow rate of 230 kg/h. To speed up this process, a Python script was developed to connect to the Aspen Plus simulation using the Aspen Plus application programming interface (API). The API is typically accessed through the *win32com* library, which allows Python to interact with COM (Component Object Model) objects. This enables backend control over the Aspen Plus simulations to run tasks and to extract desired data in an efficient manner. This facilitates the testing of various scenarios with different inputs and operational parameters without manually changing the simulation flowsheet. This proves to be a faster method than performing sensitivity analysis using the in-built Aspen tools, as the Python script allows the varying of multiple input and operational parameters at the same time. The data values from the Aspen simulation are extracted using the "Variable Explorer", and once the correct node for the desired parameter is identified, it can be modified using the script by calling onto that node. The above method is used to vary the configurations of the plug flow reactors, reaction conditions, catalyst weight, number of tubes, tube length, and tube diameter. As seen in Fig. 15, a parametric study is performed by varying the pressure in the reformer system and comparing the SMR efficiencies and methane conversion values for different average fluxes along the length of the reformer (26–32 kW/m^2). The efficiencies were

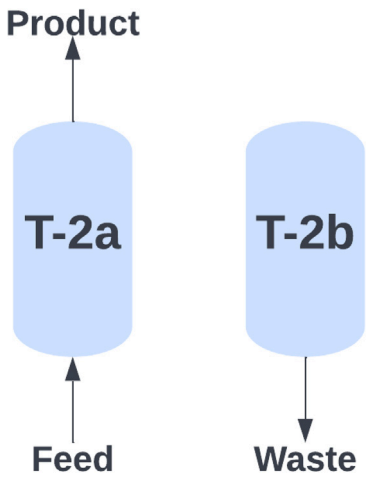

(a) Step 1: Pressurize bed 1 & Depressurize bed 2.

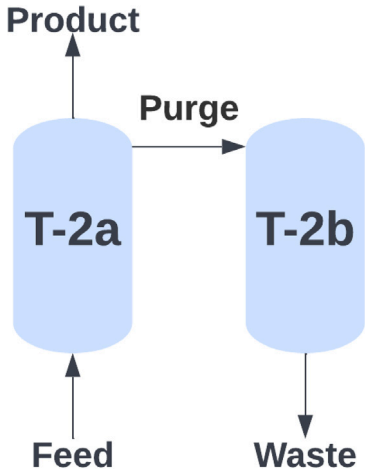

(b) Step 2: Bed 1 adsorption & Bed 2 co-current depressurization.

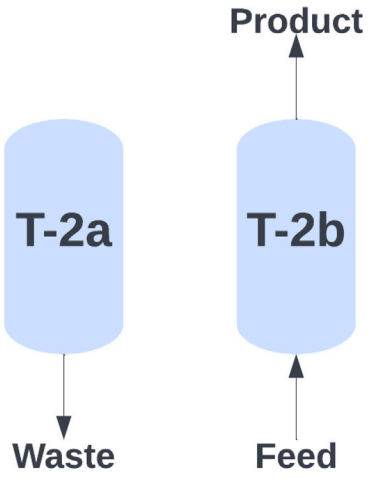

(c) Step 3: Pressurize bed 2 & Depressurize bed 1.

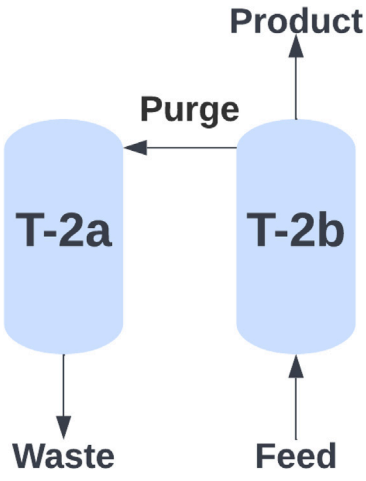

(d) Step 4: Bed 2 adsorption & Bed 1 co-current depressurization.

Fig. 11. Steps in pressure swing adsorption cycle.

calculated using Eq. (2) with the average power input to the reformer being derived from the total duty calculation in the simulation. For the total efficiency of the entire system, duties of the reformer along with the energy requirements for the pumps, multistage compressor, cooler, molecular sieve dryers, and the PSA section were taken into account. The conversion efficiency decreases with an increase in pressure, which can be attributed to lower CH_4 conversion, and consequently, lower H_2 production at elevated pressures. However, a higher pressure is necessary to maintain a suitable space velocity near 1000 h^{-1}, a linear velocity below 1.5 m/s, and a viable sizing of the reformer. For each heat flux, as the pressure of the system is modulated, the overall reformer duty is unchanged which indicates that the reformer duty is only a function of the flux. The parameter values mentioned in Table 1 were obtained after performing the given analysis and taking into account economic and practical operation limits. It was determined that the most optimal case would be a pressure of 16 bar and average heat flux around 30 kW/m^2 which results in an outlet temperature near 960 °C and a total efficiency of 78%. This specific outlet temperature is selected because of the washcoated-Ni/ZrO_2 catalyst undergoes unsustainable deactivation and sintering at temperatures above 1000 °C which imposes operational limits on such processes (Rostrup-Nielsen and Christiansen, 2011). Additionally, e-SMR is a novel process with undetermined industrial-scale energy losses. The experimental setup discussed in Section 3.2 experiences approximately 90% heat loss to the lab environment (Fig. 5(b)), however, the setup is not optimized to be thermally insulating. The reality is that electrical reforming avoids generating excess CO_2 during heating and will gain overall process efficiency with the advent of thermally insular materials with geometries suited for multitube reformers. Assuming only electrical energy inputs from non-fossil fuels, the optimal SMR and PSA Aspen model generates 5.08 kg CO_2-eq/kg H_2. This e-SMR design has the potential to decrease SMR emissions by 46% when compared to today's best available SMR technology, without carbon capture, which produces 9.00 kg CO_2-eq/kg H_2 according to the IEA (2021).

5.3. Comparative energy & emissions analysis: Conventional vs. Electrified SMR process

The traditional route to hydrogen production by way of steam methane reforming is known as the conventional SMR process. The

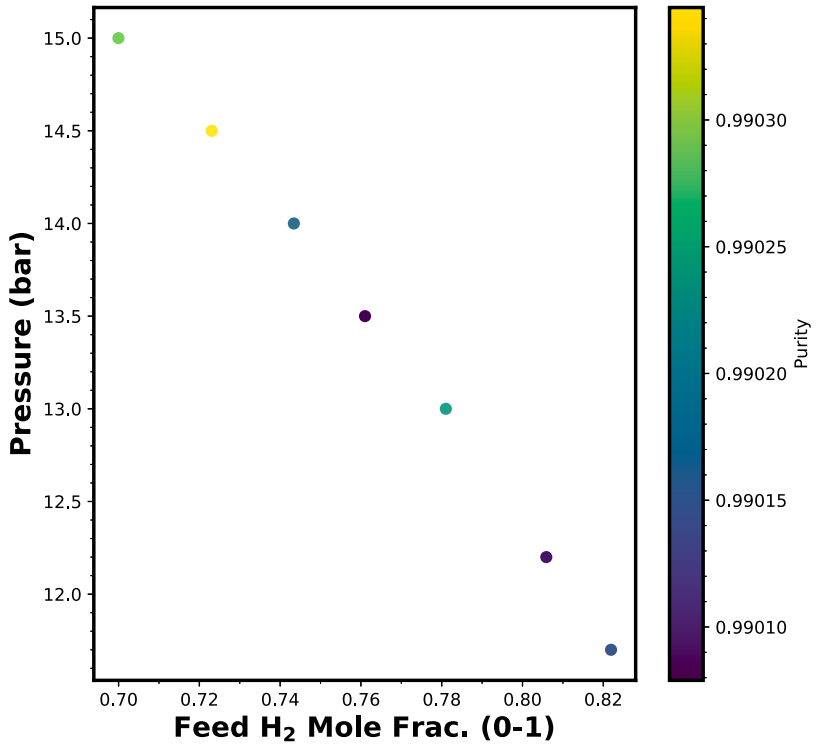

Fig. 12. PSA pressure as a function of hydrogen feed mole fraction.

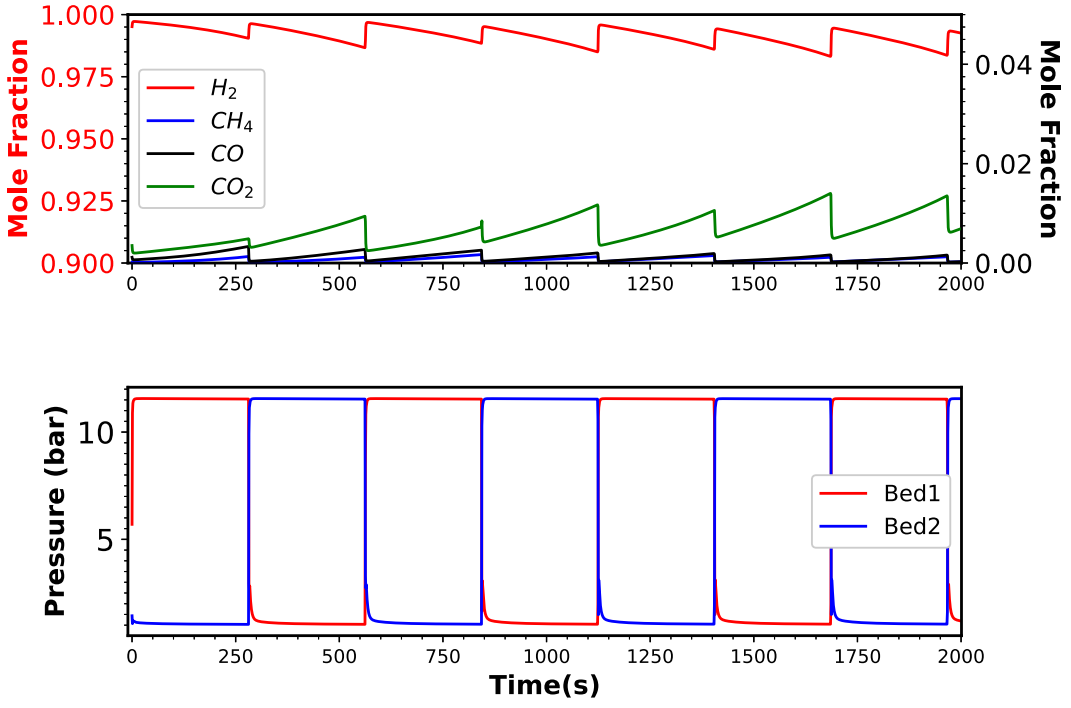

Fig. 13. Pressure swing adsorption separation performance for each outlet gas specie at the 11.7 bar pressure ceiling. The respective pressure changes in Bed T-2a and Bed T-2b for 99% H_2 purity are shown as well.

conventional process is equipped with a combustion furnace that burns natural gas to supply thermal energy to the reactor coils of the reformer unit and to chemically convert natural gas into a value-added hydrogen product. The motivation for at-scale electrified reforming processes that utilize renewable electricity is highlighted in the comparison of carbon emissions from the conventional and electrified process simulations. To that end, a conventional SMR process scheme was simulated in Aveva's Pro/II software, displayed in Fig. 16, with the simulation providing the required inputs, unit operations, and overall energy conversion to maintain the same 230 kg/h H_2 production capacity from the electrified process design. The SMR process presented in Fig. 16 is based on a real SMR process provided in Ullman's Encyclopedia of Industrial Chemistry (Ullmann, 2010). In fact, the extents of reaction, methane slip, etc. for a commercial SMR process are mentioned in the *Hydrogen,*

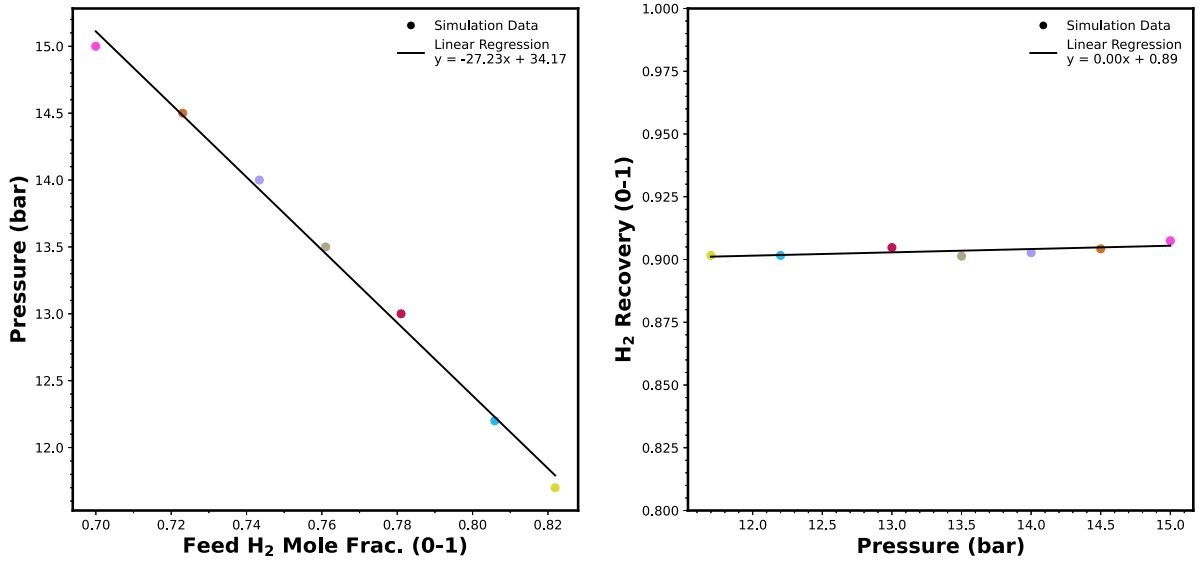

(a) H_2 fraction in the feed vs pressure needed for 99% purity separation.

(b) Pressure vs the H_2 fraction in the PSA product stream.

Fig. 14. Fitting of the simulation data for 99% purity separation, the circular markers in (a) and (b) with the same color correspond to the same data points, (a) Assuming that the feed is composed of H_2 and CO_2, the pressure needed for separation depending on the ratio of H_2 in the feed, (b) Depending on the pressure needed coming from the plot (a), the expected recovery for H_2 in the product stream. (For interpretation of the references to color in this figure legend, the reader is referred to the web version of this article.)

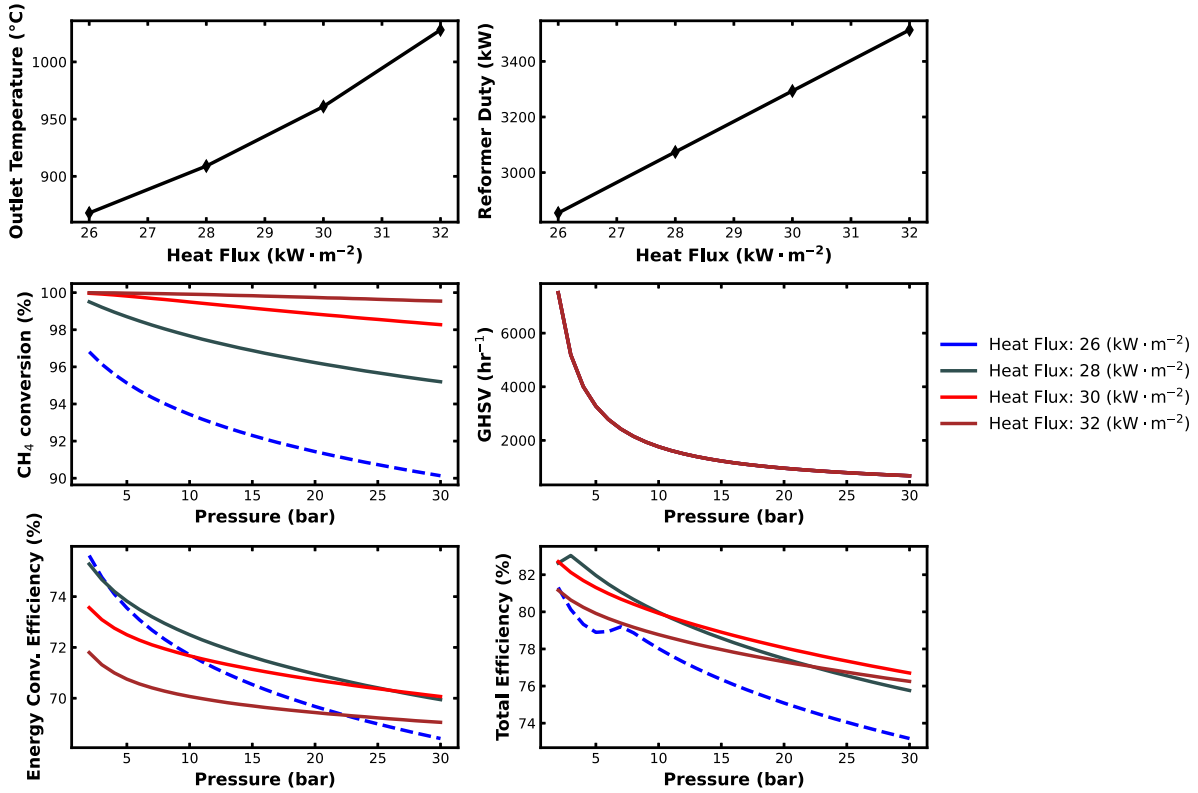

Fig. 15. Parametric study on industrial-scale Aspen simulation containing a multitube reformer with adiabatic outer walls. The sensitivity analysis explores the simulation response to a variable reformer heat flux (26–32 kW/m^2) and variable system pressure (1–30 bar). Dashed lines indicate nonviable system configurations. Solid lines indicate practical system configurations.

2. Production chapter of the aforementioned text and these parameters have been applied to this process intensification study. Two different temperatures are used for conventional and e-SMR processes because of the presence/absence of downstream WGS reactors in the two process designs. Given the e-SMR process does not have a recycle stream that combusts the unreacted CH_4, the e-SMR design requires almost full conversion of CH_4 in the reformer. The conventional SMR setup is a different process entirely that recycles unreacted CH_4 in the combustion furnace. It is true that the methane slip in the e-SMR is lower because of the reformer temperature, and it is not within the scope of this study

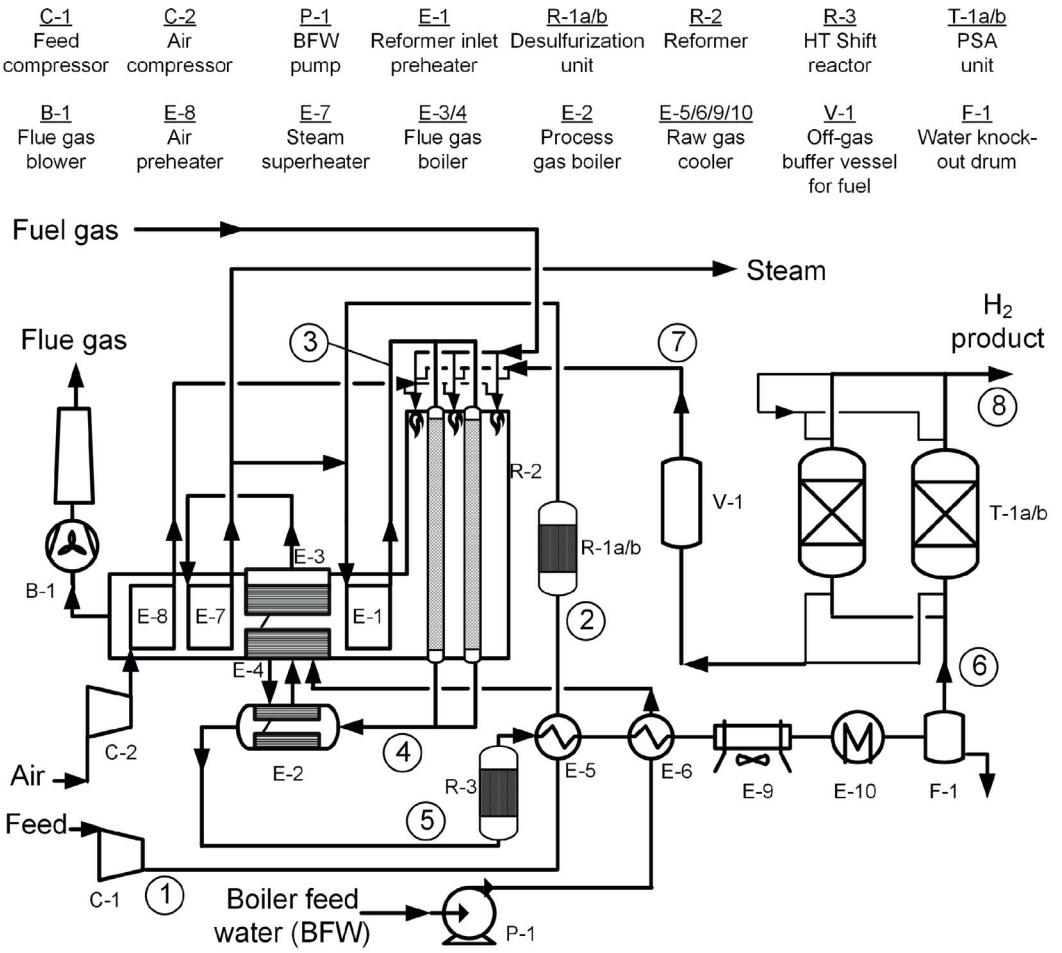

Stream No.	1	2	3	4	5	6	7	8
Mol, %	Feed	Desulfurizer inlet	Reformer inlet	Reformer outlet	HT Shift reactor inlet	PSA unit inlet	Off-gas fuel	H_2 product
H_2	0.0	0.0	0.0	52.0	52.0	74.5	37.0	99.9
Ar	0.6	0.6	0.2	0.1	0.1	0.2	0.2	0.1
CO	0.0	0.0	0.0	10.8	10.8	4.7	11.8	0.0
CO_2	1.0	1.0	0.3	5.3	5.3	15.6	38.7	0.0
CH_4	94.4	94.4	26.7	3.8	3.8	4.8	11.9	0.0
C_{2+}	3.5	3.5	1.0	0.0	0.0	0.0	0.0	0.0
H_2S	0.5	0.5	0.0	0.0	0.0	0.0	0.0	0.0
H_2O	0.0	0.0	71.9	27.9	27.9	0.2	0.4	0.0
Flowrate, m^3 (STP)/h	1054	1054	3728	5471	5471	4337	1748	2589
Mass flowrate, kg/h	799	799	2917	2917	2917	2017	1782	235
Temperature, °C	25	390	520	850	350	20	14	22
Pressure, kPa	800	1950	1900	1700	1680	1500	250	1500

Fig. 16. Conventional SMR: process flow diagram and stream table for optimized Aveva Pro/II simulation. This process also generates 2384 kg/h of superheated steam (255 °C and 3.0 MPa).

to determine the industrial-scale mass and energy distributions in two dimensions in either system. Instead, this work relies on conventional reforming case studies and an experimentally-validated kinetic model to scale each design.

The conventional H_2 production plant includes three main sections: fire-heated reforming, HT-WGS, and PSA separation. The value-added product gas is derived from a natural gas feedstock, and the furnace combusts excess compressed air and natural gas in a 3.4:1 molar ratio at 1202 °C to meet the endothermic demands of SMR reactions. The conversion of the natural gas feed to 99% purity hydrogen begins at the inlet of the process in the *Feed* stream which contains 94% CH_4. The natural gas feed is compressed from 8 to 19 bar, cooled, and desulfurized before being preheated to 390 °C to promote the cracking of longer-chain hydrocarbons into pure CH_4. After cracking, the dry natural gas is mixed with high-pressure steam at 292 °C and 19.5 bar. The wet CH_4 mixture flows from *M*1 to the conventional reformer coils that are at 850 °C to induce the chemical conversion of CH_4 and H_2O to CO, CO_2, and H_2 products. The selected extent of reaction is 0.79 (Ullmann, 2010). The remaining CO and steam react in an HT-WGS reactor at 16.8 bar and 350 °C which is modeled with a *Gibbs Reactor* model in Pro/II. The HT-WGS product mixture is flashed at 50 °C and 16.2 bar to remove water vapor from the product stream before it travels to the two-bed PSA unit held at 20 °C and 15 bar conditions. By foregoing a second low-temperature WGS reactor for the conventional SMR case,

capital costs are lessened. The conventional SMR process nears the production setpoint without needing a second WGS reactor since the reformer section can be operated at a lower operational temperature (850 °C) which still allows for the WGS reaction. Moreover, unconverted CO can be combusted in the furnace as PSA off-gas is recycled in this design. The e-SMR generates less H_2 in its reformer section given the SMR reaction dominates at a 978 °C operating temperature. A second WGS reactor is needed for the e-SMR design as a result. Following the PSA separation process for the conventional case, 2589 N m^3/h of 99% pure H_2 leaves the product stream. The PSA off-gas is recycled to the combustion furnace fuel stream at a rate of 79.8 kmol/h. The CO_2 emission rate in the flue-gas stream that exits the combustion furnace is 53 kmol/h, compared to the electrified process that emits CO_2 at a 26.6 kmol/h rate. As predicted, the electrified SMR process saves roughly 50% in CO_2 emissions, assuming all the energy supplied to the process is sourced from low-to-no-carbon electricity.

Regarding the integrity of the nickel chromium alloy that is used in experiments, the maximum operating temperature per Goodfellow's technical data sheet is 1100–1300 °C. The tensile strength of a 6 mm outer diameter (OD) X 500 mm length FeCrAl tube is 500 bar. Sandmeyer Steel's 310 Alloy is also a FeCr alloy and has a 1000 h creep strain of 3 MPa at 1000 °C which translates to a safe operational pressure of 17.4 bar if the OD of the optimized reformer is 18 mm with an ID of 9.9 mm. If the operational temperature was around 800 °C, as seen in the conventional reforming case, the e-SMR tubes only require an outer diameter of 11.79 mm which would save considerably more material. It needs to be said, however, that commercial SMR furnaces have materials that withstand temperatures in excess of 1200 °C at elevated-pressures. The material cost for the e-SMR reformer that operates at 978 °C, therefore, is no different than the cost of materials in the conventional furnace, from a metallurgical standpoint.

Heat integration in the conventional SMR process has additional complexities due to the availability of recoverable energy in the flue gas stream that exits the furnace and originates from the combustion of CH_4 at 1200 °C. A total of eight heat exchangers and two coolers are used for the Pro/II simulation in Fig. 16, and the temperature of the flue gas stream is decreased from 1200 to 200 °C by transferring thermal energy to the high pressure steam feed for reforming, the process gas feed for pre-reforming, and the compressed air feed (Fig. 17(a)). The post-reformer effluent is also used to generate high pressure steam. Overall, 5.1 MW of thermal energy is recovered from heat exchange network and 0.8 MW is lost through cooling utilities. Though the conventional heat exchanger network recovers a larger amount of heat, the electrified system loses 0.7 MW to cooling utilities (Fig. 17(b)). The electrified system also requires half the number of heat exchanger units which helps to lower the additional capital cost incurred from the need for a LT-WGS reactor. Two Sankey diagrams in Fig. 18 map the energy inputs of both process designs to their respective energy outputs. The natural gas feed requirement is 19.9 GJ/h greater for the conventional reforming design to fuel its distinctive combustion reaction, and an additional 6.4 GJ/h input is needed overall for this classical reforming scenario. The electrified reforming design produces more H_2 product and has fewer thermal losses when compared to the conventional design under similar conditions. Another distinction between the two reformation models, from an energy standpoint, is the lack of a PSA off-gas recycle for the e-SMR design, understanding that the electrified process does not have a furnace to which off-gas can be burned. Still, both designs have similar energy utilization and loss, so the primary justification for an electrified reforming system lies in its potential to significantly reduce carbon emissions.

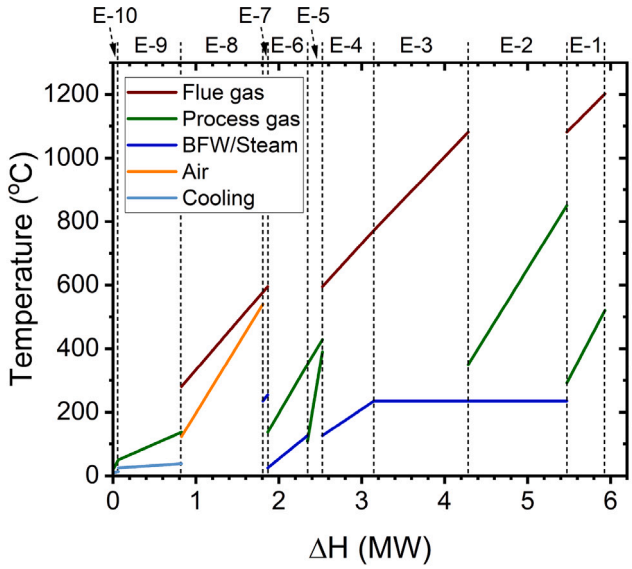

(a) Conventional SMR: heat exchanger enthalpies.

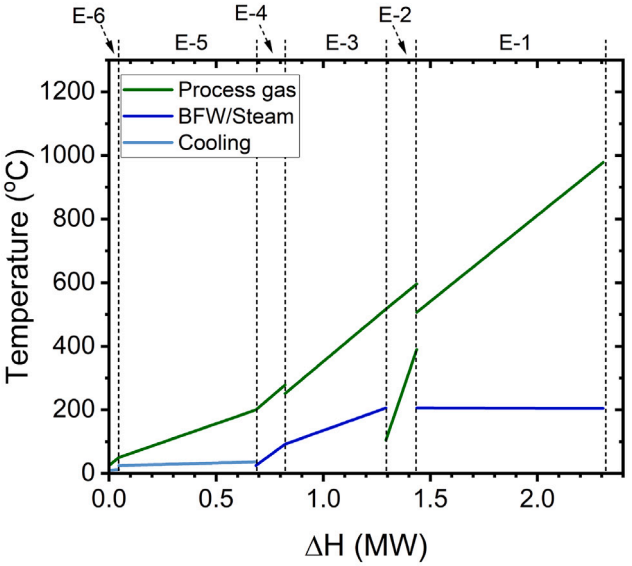

(b) Electrified SMR: heat exchanger enthalpies. Heat integration values correspond to the the overall process flowsheet in Fig. 8

Fig. 17. Heat duty curves for conventional and electrified SMR process designs.

6. Conclusion

The SMR process is the cornerstone of industrial H_2 production. Despite its widespread adoption, traditional SMR processes rely on fossil fuels for supplying heat energy, contributing significantly to greenhouse gas emissions. Motivated by a need to change the way heat is supplied to SMR processes, this work focused on an electrically-heated steam methane reformer process, and using experimental results from an electrically-heated steam methane reformer at UCLA, the process was initially modeled with industrial process simulators. Average flux values were configured to match experimental reformer temperatures, space velocities, and pressures to compare the ideal kinetic energy consumption of the reformer to experimental energy data. Based on these data, an Aspen Plus model was constructed and tailored for an industrial-scale hydrogen production process. Subsequently, Aspen Adsorption software was used to model the PSA process that filters high-purity hydrogen. PSA simulation data was fit to curves for fast separations calculations that permitted the integration of the PSA simulation into the entire SMR-PSA plant model. Finally, a sensitivity analysis was performed to identify energy-efficient operating conditions and compare the conventional SMR process versus the electrified SMR process.

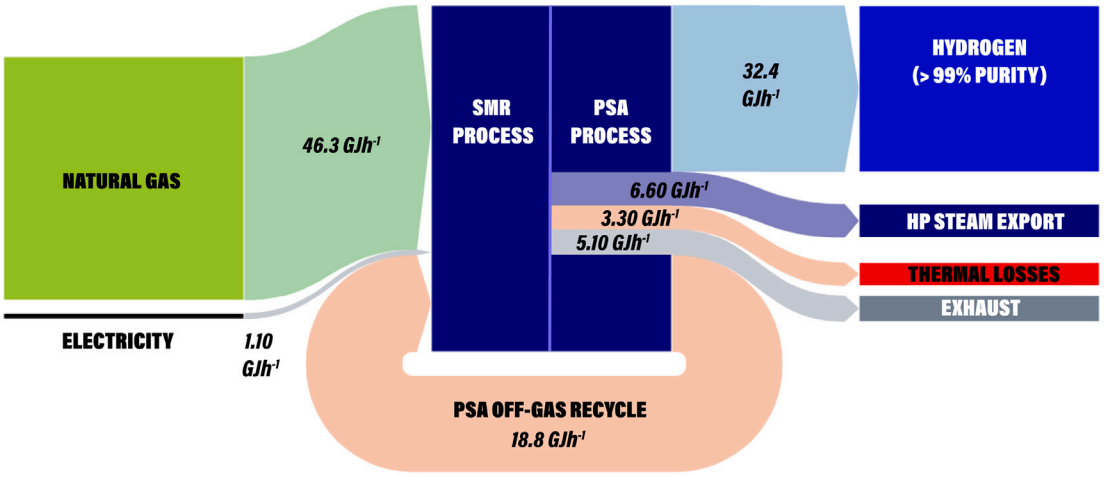

(a) Conventional SMR with natural gas feeds for SMR reactions and combustion heating to generate a 230 kg/h H_2 production rate.

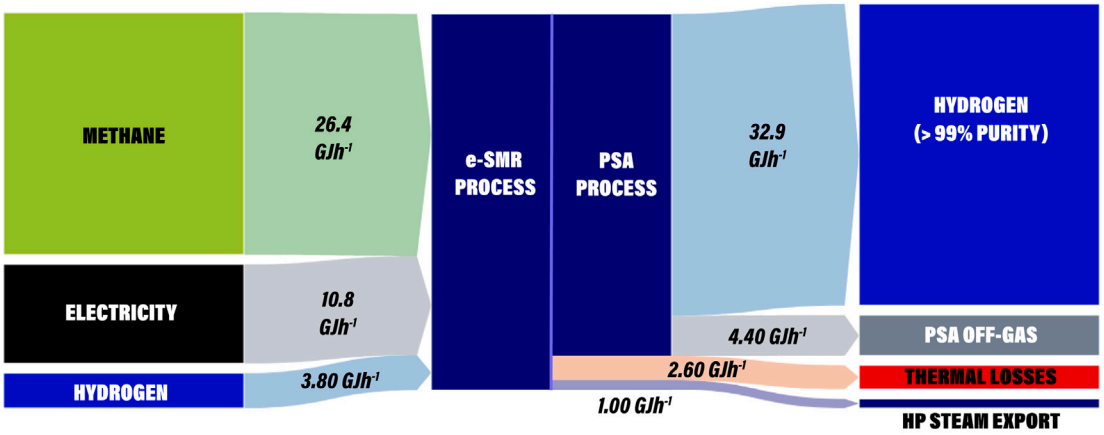

(b) Electrified reforming process with a pure CH_4 feed and a 231 kg/h H_2 production rate.

Fig. 18. Energy utilization diagrams for conventional and electrified processes.

CRediT authorship contribution statement

Esther Hsu: Conceptualization, Investigation, Methodology, Writing – original draft. **Dominic Peters:** Conceptualization, Investigation, Methodology, Writing – original draft. **Berkay Çıtmacı:** Conceptualization, Investigation, Methodology, Writing – original draft. **Parth Chheda:** Investigation, Conceptualization, Methodology. **Xiaodong Cui:** Investigation, Software. **Yifei Wang:** Software. **Carlos G. Morales-Guio:** Conceptualization, Funding acquisition, Methodology, Supervision, Writing – original draft, Writing – review & editing. **Panagiotis D. Christofides:** Conceptualization, Funding acquisition, Supervision, Writing – review & editing, Methodology, Writing – original draft.

Declaration of competing interest

The authors declare that they have no known competing financial interests or personal relationships that could have appeared to influence the work reported in this paper.

Acknowledgments

We would like to gratefully acknowledge financial support from the U.S. Department of Energy, through the Office of Energy Efficiency and Renewable Energy (EERE), under the Advanced Manufacturing Office Award Number DE-EE0007613.

References

Ahn, H., Chun, C., Park, M., Ahn, I.-S., Lee, C.-H., 2001. Thermal effects on the breakthrough curve of a hydrogen ternary system at a fixed bed. Sep. Sci. Technol. 36, 2121–2145.

Ahn, S., You, Y.-W., Lee, D.-G., Kim, K.-H., Oh, M., Lee, C.-H., 2012. Layered two-and four-bed PSA processes for h_2 recovery from coal gas. Chem. Eng. Sci. 68, 413–423.

Ashik, U.P.M., Wan Daud, W.M.A., Abbas, H.F., 2017. Methane decomposition kinetics and reaction rate over Ni/SiO_2 nanocatalyst produced through co-precipitation cum modified Stöber method. Int. J. Hydrog. Energy 42, 938–952.

Bartholomew, C.H., Farrauto, R.J., 2011. Fundamentals of Industrial Catalytic Processes. John Wiley & Sons.

Chen, W.-H., Chen, C.-Y., 2020. Water gas shift reaction for hydrogen production and carbon dioxide capture: A review. Appl. Energy 258, 114078.

Çıtmacı, B., Cui, X., Abdullah, F., Richard, D., Peters, D., Wang, Y., Hsu, E., Chheda, P., Morales-Guio, C.G., Christofides, P.D., 2024a. Model predictive control of an electrically-heated steam methane reformer. Digit. Chem. Eng. 10, 100138.

Çıtmacı, B., Peters, D., Cui, X., Abdullah, F., Almunaifi, A., Chheda, P., Morales-Guio, C.G., Christofides, P.D., 2024b. Feedback control of an experimental electrically-heated steam methane reformer. Chem. Eng. Res. Des. 206, 469–488.

Cui, X., Çıtmacı, B., Peters, D., Abdullah, F., Wang, Y., Hsu, E., Chheda, P., Morales-Guio, C.G., Christofides, P.D., 2024. Estimation-based model predictive control of an electrically-heated steam methane reforming process. Digit. Chem. Eng. 11, 100153.

Do, T.N., Kwon, H., Park, M., Kim, C., Kim, Y.T., Kim, J., 2023. Carbon-neutral hydrogen production from natural gas via electrified steam reforming: Techno-economic-environmental perspective. Energy Convers. Manage. (ISSN: 0196-8904) 279, 116758.

DOE, 1997. Saving Energy with Electrical Resistance Heating. Department of Energy Report, https://www.nrel.gov/docs/legosti/fy97/6987.pdf.

Du, Z., Liu, C., Zhai, J., Guo, X., Xiong, Y., Su, W., He, G., 2021. A review of hydrogen purification technologies for fuel cell vehicles. Catalysts 11, 393.

Dunikov, D., Borzenko, V., Blinov, D., Kazakov, A., Lin, C.-Y., Wu, S.-Y., Chu, C.-Y., 2016. Biohydrogen purification using metal hydride technologies. Int. J. Hydrog. Energy 41, 21787–21794.

Gabelman, P., 2017. Adsorption basics: part 2. Chem. Eng. Prog. 113 (8), 38–45.

Ginsburg, J.M., Piña, J., El Solh, T., de Lasa, H.I., 2005. Coke formation over a nickel catalyst under methane dry reforming conditions: Thermodynamic and kinetic models. Ind. Eng. Chem. Res. 44, 4846–4854.

Grande, C.A., 2012. Advances in pressure swing adsorption for gas separation. Int. Sch. Res. Not. 2012, 982934.

Häussinger, P., Lohmüller, R., Watson, A.M., 2011. Hydrogen, 2. Production. In: Ullmann's Encyclopedia of Industrial Chemistry. John Wiley & Sons, Ltd, ISBN: 9783527306732.

IEA, 2021. Comparison of the emissions intensity of different hydrogen production routes. https://www.iea.org/data-and-statistics/charts/, (Accessed on 24 June 2024).

Ivanov, Y., Pyatnichko, O., Zhuk, H., Onopa, L., Soltanibereshne, M., 2017. Extraction of carbon dioxide from gas mixtures with amines absorbing process. Energy Procedia 128, 240–247.

Kashid, M.N., Renken, A., Kiwi-Minsker, L., 2014. Microstructured Devices for Chemical Processing. John Wiley & Sons.

Klopčič, N., Grimmer, I., Winkler, F., Sartory, M., Trattner, A., 2023. A review on metal hydride materials for hydrogen storage. J. Energy Storage 72, 108456.

Kumar, A., Baldea, M., Edgar, T.F., 2016. Real-time optimization of an industrial steam-methane reformer under distributed sensing. Control Eng. Pract. 54, 140–153.

Li, P., Wang, Z., Qiao, Z., Liu, Y., Cao, X., Li, W., Wang, J., Wang, S., 2015. Recent developments in membranes for efficient hydrogen purification. J. Membr. Sci. 495, 130–168.

Linde-Engineering, 2024. Hydrogen recovery by pressure swing adsorption.

Luberti, M., Ahn, H., 2022. Review of polybed pressure swing adsorption for hydrogen purification. Int. J. Hydrog. Energy 47 (20), 10911–10933.

Lubitz, W., Tumas, W., 2007. Hydrogen: An overview. Chem. Rev. 107, 3900–3903.

Mendes, D., Chibante, V., Mendes, A., Madeira, L.M., 2010. Determination of the low-temperature water-gas shift reaction kinetics using a Cu-based catalyst. Ind. Eng. Chem. Res. 49, 11269–11279.

Molburg, J.C., Doctor, R.D., 2003. Hydrogen from steam-methane reforming with CO_2 capture. In: Proceedings of 20th Annual International Pittsburgh Coal Conference. Pittsburgh, PA, USA, pp. 1–21.

Panchenko, V., Daus, Y.V., Kovalev, A., Yudaev, I., Litti, Y.V., 2023. Prospects for the production of green hydrogen: Review of countries with high potential. Int. J. Hydrog. Energy 48, 4551–4571.

Park, D., Duffy, G., Edwards, J., Roberts, D., Ilyushechkin, A., Morpeth, L., Nguyen, T., 2009. Kinetics of high-temperature water-gas shift reaction over two iron-based commercial catalysts using simulated coal-derived syngases. Chem. Eng. J. 146, 148–154.

Rase, H.F., 1977. Chemical Reactor Design for Process Plants; Volume Two: Case Studies and Design Data. John Wiley & Sons.

Rostrup-Nielsen, J., Christiansen, L.J., 2011. Concepts in Syngas Manufacturing, vol. 10, World Scientific.

Ruthven, D.M., Farooq, S., Knaebel, K.S., 1996. Pressure Swing Adsorption. John Wiley & Sons.

Sazali, N., 2020a. A comprehensive review of carbon molecular sieve membranes for hydrogen production and purification. Int. J. Adv. Manuf. Technol. 107, 2465–2483.

Sazali, N., 2020b. A review of the application of carbon-based membranes to hydrogen separation. J. Mater. Sci. 55, 11052–11070.

Sircar, S., Golden, T.C., 2000. Purification of hydrogen by pressure swing adsorption. Sep. Sci. Technol. 35, 667–687.

Skarstrom, C.W., 1963. Timing cycle for improved heatless fractionation of gaseous materials. US Patent 3, 104, 162.

Song, C., Liu, Q., Deng, S., Li, H., Kitamura, Y., 2019. Cryogenic-based CO_2 capture technologies: State-of-the-art developments and current challenges. Renew. Sustain. Energy Rev. 101, 265–278.

Terrigeol, A., Trifilieff, O., 2015. Practical considerations for the design of adsorbent beds–molecular sieve lifetime optimization. In: Gas Processors Association 23rd Annual Technical Conference. La Garenne Colombes, France.

Ullmann, 2010. Encyclopedia of Industrial Chemistry. Wiley-VCH, Weinheim.

Wang, P., Chen, Y., Teng, Y., An, S., Li, Y., Han, M., Yuan, B., Shen, S., Chen, B., Han, S., et al., 2024. A comprehensive review of hydrogen purification using a hydrate-based method. Renew. Sustain. Energy Rev. 194, 114303.

Wiheeb, A., Helwani, Z., Kim, J., Othman, M., 2016. Pressure swing adsorption technologies for carbon dioxide capture. Sep. Purif. Rev. 45, 108–121.

Wismann, S.T., Engbæ k, J.S., Vendelbo, S.r.B., Bendixen, F.B., Eriksen, W.L., Aasberg-Petersen, K., Frandsen, C., Chorkendorff, I., Mortensen, P.M., 2019. Electrified methane reforming: A compact approach to greener industrial hydrogen production. Science 364, 756–759.

Wood, K.R., Liu, Y.A., Yu, Y., 2018. Design, Simulation and Optimization of Adsorptive and Chromatographic Separations: A Hands-On Approach. John Wiley & Sons.

Xu, J., Froment, G.F., 1989. Methane steam reforming, methanation and water-gas shift: I. Intrinsic kinetics. AIChE J. 35, 88–96.